Metal oxide redox chemistry for chemical looping processes

Liang Zeng[1,4], Zhuo Cheng[2,4], Jonathan A. Fan[3], Liang-Shih Fan[2] and Jinlong Gong[1]**

Abstract | Chemical looping offers a versatile platform to convert fuels and oxidizers in a clean and efficient manner. Central to this technology are metal oxide materials that can oxidize fuels, affording a reduced material that can be reoxidized to close the loop. Recent years have seen substantial advances in the design, formulation and manufacture of these oxygen carrier materials and their incorporation into chemical looping reactors for the production of various chemicals. This Review describes the mechanisms by which oxygen carriers undergo redox reactions and how these carriers can be incorporated into robust chemical looping reactors.

It is desirable to perform energy or materials conversions through small, clean, safe and energy-efficient process technologies. One means toward this process intensification is chemical looping, whereby a reaction or separation can be broken down into multiple subreactions that take place in isolated steps or spaces[1]. Chemical looping involves the reaction and regeneration of chemical intermediates, such as metal oxides (MO_x) that can oxidize feedstocks before being reoxidized in a separate reaction (FIG. 1Aa). This process is generally referred to as chemical looping full oxidation (CLFO), a particular case of which is chemical looping combustion (CLC), a stepwise concept that enables efficient CO_2 capture — an attractive prospect in light of growing concerns over greenhouse gas emissions from coal-fired power plants[2,3]. The corresponding intermediates are necessarily recyclable oxygen carriers such as FeO_x and CuO (REFS[4–8]). A CLC process involves fuel combustion taking place in two interconnected reactors: a reducer (or fuel reactor) and an oxidizer (also referred to as a combustor or air reactor). In the reducer, oxygen carriers donate O atoms from their lattice to effect complete oxidation of fuel to CO_2 and H_2O, readily affording a high-purity CO_2 stream after the removal of H_2O by condensation. The reduced (deoxygenated) oxygen carrier is then regenerated in the oxidizer using air, with the heat thus released being used for steam and electricity generation. This flameless overall combustion, in which the fuel never contacts air, affords far less dioxins and NO_x by-products than conventional combustion[9,10]. In addition, CLC gives rise to low process irreversibility because it enables the recuperation of low-grade heat in the low-temperature endothermic reduction step while producing more high-grade heat in the high-temperature oxidation step. In this way, CLC can result in superior exergy efficiency relative to conventional combustion[11]. The CLC approach obviates the mixing of air and fuel and directly generates a concentrated CO_2 stream. This occurs without the need for the energy-intensive and cost-intensive air separation unit or acid gas removal unit required in other CO_2 capture technologies. When combined with advanced ultra-supercritical technologies, CLC is considered one of the most promising electric power generation techniques for carbon-constrained scenarios[12–14].

One variant of the CLFO and CLC approaches for oxidation is chemical looping with oxygen uncoupling (CLOU), whereby the oxidized carrier is thermolyzed to liberate O_2, which then assists in situ fuel oxidation or reacts with the fuel in an additional step not involving the carrier[15]. In the latter route, the carrier is never exposed to the fuel and is thus not susceptible to processes such as coking. In addition to these applications, oxygen carriers are used in chemical looping partial oxidation[14] (CLPO; FIG. 1Ab). The major difference between CLFO and CLPO is that the former converts hydrocarbons into high-purity CO_2 with the release of thermal energy, while the latter aims for improved yields of CO and/or H_2. In contrast to conventional fossil fuel gasification and reforming processes, CLPO eliminates the need for an air separation unit, water–gas shift reactor and acid gas removal unit. CLPO has the potential to directly generate high-quality syngas with desirable H_2:CO ratios and lower CO_2 content[16–21]. Fundamental research on the use of CLPO schemes has also been conducted in renewable energy systems such as those involving the thermochemical splitting of CO_2/H_2O to produce CO/H_2 and O_2 (REFS[22–25]) (FIG. 1Ac). Another similar oxidative approach is chemical looping selective oxidation (CLSO; FIG. 1Ad), which can be applied to the manufacture of valuable chemicals if the oxygen carriers feature catalytic sites or can host external dedicated catalysts. The CLSO scheme requires a distinct overall reaction path that involves lattice oxygen as well as catalytic sites that enable high

[1]*Key Laboratory for Green Chemical Technology of Ministry of Education, School of Chemical Engineering and Technology, Tianjin University, Collaborative Innovation Center of Chemical Science and Engineering, Tianjin, China.*

[2]*William G. Lowrie Department of Chemical and Biomolecular Engineering, Ohio State University, Columbus, OH, USA.*

[3]*Department of Electrical Engineering, Ginzton Laboratory, Spilker Engineering and Applied Sciences, Stanford University, Stanford, CA, USA.*

[4]*These authors contributed equally: Liang Zeng, Zhuo Cheng.*

**e-mail: fan.1@osu.edu; jlgong@tju.edu.cn*

https://doi.org/10.1038/s41570-018-0046-2

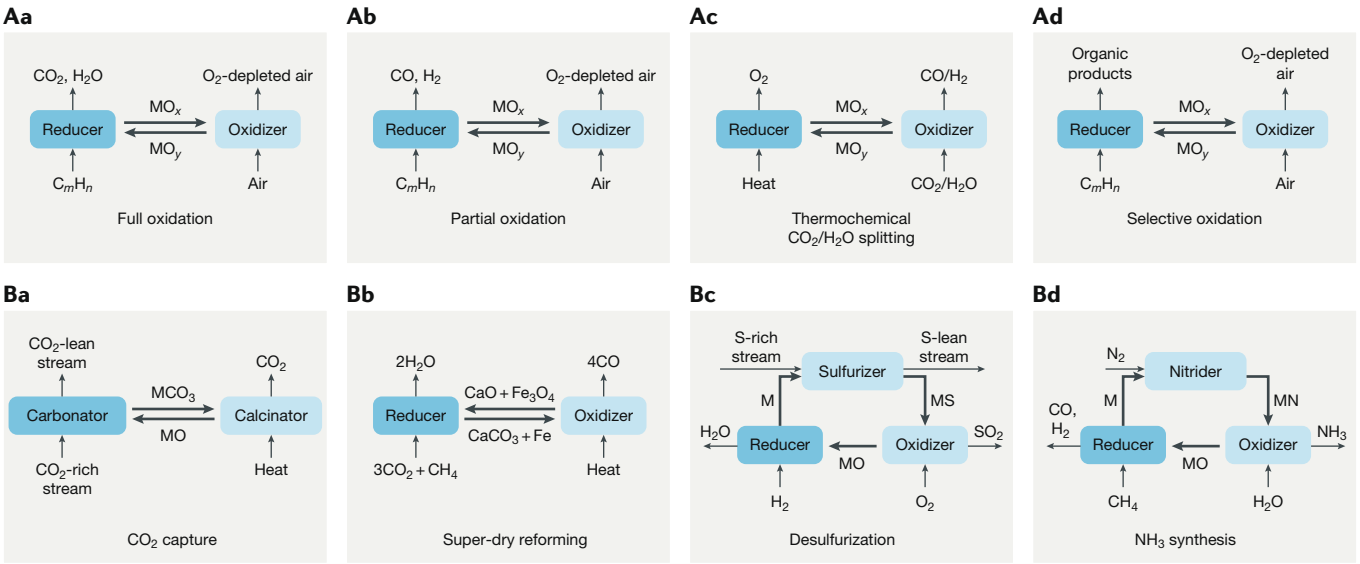

Fig. 1 | **Chemical looping involves exposing a solid carrier material to different feed streams in separate steps.** **A** | Overall oxidation reactions involve transporting oxygen carriers MO_x and MO_y ($x<y$) to an oxidizer and a reducer, respectively. **Aa** | One example of full aerobic oxidation is combustion of a hydrocarbon C_mH_n, which can also take place with the uncoupling of O_2 (REFS[1,2]). **Ab** | Partial oxidation of C_mH_n (or gasification of C) affords syngas[14,21]. **Ac** | Chemical looping can also be used to effect the thermochemical splitting reactions $CO_2 \rightleftharpoons CO + ½O_2$ and $H_2O \rightleftharpoons H_2 + ½O_2$ (REFS[24,25]). **Ad** | Selective oxidation of hydrocarbon feeds can afford value-added products, including higher alkanes, alkenes and epoxides[26,27]. **B** | Solid materials can also carry other groups between separate reactors. **Ba** | MO can reversibly trap CO_2 to afford MCO_3, thereby allowing the concentration of CO_2 (REF.[28]). **Bb** | Hybrid looping, using both a CO_2 carrier and an O atom carrier, allows for so-called super-dry reforming[8]. **Bc** | Using a combination of Ni and Zn (to carry O and S, respectively), one can construct a hybrid looping process for desulfurization[29]. **Bd** | Another hybrid loop featuring three reactors enables the synthesis of NH_3 (REFS[30,31]). The steps in a chemical loop occur sequentially, but the same reactor can potentially be used for each step. The arrows between the reactors denote the form of the carrier that is generated in one step and used in the next.

activity and selectivity. One early example of CLSO is the DuPont process for converting butane into maleic anhydride, a reaction catalysed by vanadium phosphorous oxide (VPO), which can repeatedly donate and accept O atoms in a circulating fluidized bed reactor[26,27].

Chemical looping technology is not restricted to (overall) oxidation reactions, and if one uses oxygen carriers with other carrier materials, one can realize a broad reaction scope. A simple example is the aforementioned use of CaO as a carrier to concentrate CO_2 (FIG. 1Ba) during pre-combustion or post-combustion capture[28]. For example, a CO_2 carrier such as CaO/Al_2O_3, when complemented with $Fe_3O_4/MgAl_2O_4$ as an oxygen carrier and $Ni/MgAl_2O_4$ as a CH_4 reforming catalyst, enables the 'super-dry' reforming process for the production of pure CO from CH_4 and CO_2 (REF.[8]) (FIG. 1Bb). Using Ni and Zn materials as oxygen and sulfur carriers, respectively, Phillips developed the S-Zorb process to substantially lower the S content in gasoline while preserving high-octane olefins and aromatics[29] (FIG. 1Bc). Our last introductory example is the realization of the Haber–Bosch process through chemical looping, whereby both oxygen and nitrogen carriers handle H_2O, CH_4 and N_2 to afford NH_3 along with CO and H_2 (REFS[30,31]) (FIG. 1Bd).

Despite the contrasting applications of the above chemical looping schemes, each is designed to optimize the material and energy distribution with intensified process performance, resulting in lower costs, emissions and energy penalties. This Review surveys recent research in the redox chemistry of oxygen carriers in the context of chemical looping, work that is motivated by our need for clean and efficient schemes for material and energy conversions. We pay particular attention to state-of-the-art CLC systems (FIG. 1A) before describing the newer areas of CLPO and CLSO, all the while focusing on the questions and guidelines regarding the design of new oxygen carriers and chemical looping reactions.

Chemical looping process development

The concept of chemical looping was introduced in the 19th century (FIG. 2) with the development of an air separation process by Quentin and Arthur Brin[32]. In the Brin process, the equilibrium $BaO + ½O_2 \rightleftharpoons BaO_2$ is manipulated by subjecting fixed BaO/BaO_2 bed retorts to cycles of temperature and pressure swings. During 1886–1906, the Brin's Oxygen Company used this method to isolate O_2, although their method was later superseded by the fractionation of liquid air[33]. Another early study involved the use of a redox chemical looping process to produce CaC_2. Developed in 1897, this process makes use of a reducer, in which a hydrocarbon fuel (coal, coke or liquid hydrocarbons) and CaO convert MnO_2 into Mn(II,III) oxides. The O atoms are used in the combustion of the fuel, while the Mn(II,III) oxides are reoxidized to MnO_2 in a separate air reactor[34]. Later work in the 1950s saw the use of Fe/Cu oxides as oxygen

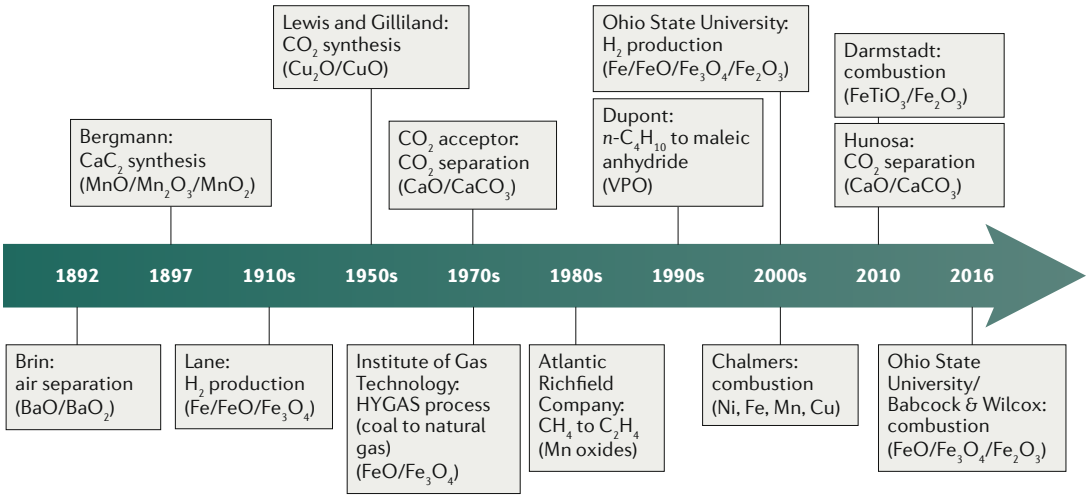

Fig. 2 | **Selected developments in chemical looping for combustion, partial oxidation and selective oxidation.** The solid materials used as carriers are shown in parentheses[26,27,32–39,43,47,49,59–65].

carriers to generate CO_2 for the beverage industry. The CO_2 arises from the reaction of a metal oxide with a fuel in a reducer, which can take the form of a multistage fluidized bed, stoker-type or moving bed design with a gas–solid countercurrent flow pattern[35,36]. In the 1970s, the Institute of Gas Technology developed the HYGAS process to convert coal into synthetic natural gas over a material that is cycled between reduced (FeO) and oxidized (Fe_3O_4) states. The reducer and oxidizer in this looping scheme are two-stage countercurrent fluidized bed reactors — a setup that improves the fuel gas and Fe oxide conversions as well as heat and mass transfer[37]. The term chemical looping combustion was introduced in the 1980s in the context of improving the efficiency of an irreversible heat engine using metal oxide redox cycles[38]. CLFO and CLC have also found uses beyond the direct production of high-purity O_2 or CO_2. Over the past two decades, various CLC processes have been quickly developed and demonstrated at bench to pilot scales, taking advantage of in situ CO_2 separation, with a circulating fluidized bed design being widely used[2,5]. Many of these projects have involved extensive cooperation between universities and energy companies to industrialize CLC technologies. For example, a dual circulating fluidized bed system design, in combination with ilmenite ore ($FeTiO_3$) as oxygen carriers, is exploited in a thermal-megawatt-scale (1 MW_{th}) coal-fuelled CLC pilot plant at the Technical University of Darmstadt[39]. The University of Utah and SINTEF Energy Research also capture CO_2 but instead make use of Cu_2O-based and CuO-based CLOU processes, in which CuO liberates O_2 in the reducer to increase the gasification rate of solid fuels[40,41]. Limestone-based CLC uses $CaSO_4$ as an oxygen carrier that passes between two fast circulating fluidized bed reactors[42]. Other such projects include a 3 MW_{th} coal direct chemical looping pilot between Ohio State University and Babcock & Wilcox (USA) and a 75 MW_{th} circulating fluidized bed boiler operation in an oxygen-carrier-aided combustion system by Chalmers University of Technology (Sweden) and E.ON[43,44]. Similarly, Southeast University and Tsinghua University (China) are teaming up with different industrial partners to develop two separate 3 MW_{th} CLC pilot plants[13,45,46]. These large pilot tests serve to demonstrate the feasibility of CLC under industrial conditions and will allow us to identify technology gaps that must be addressed before carrying out a further scale-up.

The CLPO approach is relatively new in that its application can only be traced back to the early 1900s, when fixed beds filled with Fe ore were exposed to successive cycles of syngas and steam for the commercial production of H_2 (REF.[47]). In the 1950s, fluidized beds were used for CLPO to increase the contact between steam and solid Fe oxide[48]. The 1970s saw the development of the CO_2 acceptor gasification process, whereby coal was converted into synthetic natural gas using a gasifier featuring CaO for both the in situ removal of CO_2 and enrichment of H_2 through the shifted water–gas shift reaction[49].

Studies in thermochemical H_2O and CO_2 splitting began to emerge in the 1980s, and since then, a series of thermochemical cycles have been examined[25,50–52]. In the 1990s, it was found that lattice O atoms from Ce oxides can participate in the partial oxidation of CH_4 to syngas[53,54]. A further proposal described how solar energy can provide heat to drive the partial oxidation of CH_4 to syngas over fluidized Fe oxides, and chemical looping reforming would later develop along a similar vein[5,55,56]. The recent realizations of CLC technology, at least on the pilot plant scale, have also seen CLPO attract more research attention. General Electric and Alstom have independently studied a three-reactor system circulated with both oxygen carriers and carbon dioxide carriers to process coal and produce H_2 (REFS[42,57]). More recently, as of 2018, the ENN Energy Research Institute (China) is scaling up a 1 MW_{th} chemical looping gasification pilot unit for the efficient production of H_2-rich syngas[58]. Concurrently, Ohio State University is demonstrating a high-pressure syngas chemical looping pilot plant that runs on coal-derived syngas and natural gas feedstocks to produce H_2 (REF.[59]). The reducer and oxidizer in this plant are moving beds, with the combustor

being a fluidized bed. Ohio State University is also scaling up coal-to-syngas and shale-gas-to-syngas processes at bench and sub-pilot scales[16,60–62]. Overall, these developments in CLPO technology are principally motivated by pressing needs for cost-effective and energy-effective production of high-purity H_2 and/or CO.

Related to CLPO is CLSO, an approach that has several potential applications in chemical synthesis — not the least of which is the direct conversion of light alkanes to obtain valuable olefins and aromatics. CLSO has its origins in the early 20th century, with the development of endothermic thermal cracking and pyrolysis as well as exothermic catalytic oxidation[14,63]. Thermal cracking reactions usually require high temperatures, which add to the process cost and limit product yields owing to the trade-off between thermodynamic equilibrium and coke formation. These deleterious effects can be partially avoided by selectively reacting H_2 and O_2 over the metal oxide catalysts, but this can also cause deep gas-phase oxidation of a hydrocarbon feedstock to CO_x, decreasing selectivities for the partially oxidized products and creating hot spots when this co-feeding mode is adopted. These problems can be solved by decorating oxygen carriers with catalytic active sites and tuning the nature of the surface oxygen species. Union Carbide first proposed the oxidative coupling of methane (OCM) for direct C_2H_4 synthesis in 1982 (REF.[64]), a process that would later be adapted by the Atlantic Richfield Company to proceed over a redox fast fluidized bed[65]. The OCM process has recently been improved by using a Mn-based and Mg-based catalytic oxygen carrier, which is stable for 100 cycles with a 63.2% C2 selectivity and 23.2% yield[66]. One can also convert CH_4 into higher hydrocarbons such as C_6H_6 by using Mo/H-ZSM-5 as a dehydroaromatization catalyst. The H_2 generated by this process is used to reduce Fe_3O_4 to FeO, with the H_2O byproduct being trapped by a zeolite[67]. Thus, a chemical loop that can afford aromatics in yields as high as 43% is established, with the products being inherently free of H_2 on account of Fe_3O_4–FeO serving as an oxygen carrier. More recently, Cu-exchanged mordenite zeolite has been used to oxidize CH_4 to methoxy intermediates, with the zeolite then recovering O from H_2O while directly producing CH_3OH (~97% selectivity) and H_2 (REF.[68]). However, the reaction of CH_4 and H_2O to generate CH_3OH and H_2 is thermodynamically unfavourable at any temperature such that even if the reaction is separated into two steps, it seems inconceivable to carry out the net reaction in a practical manner. Despite this hinderance, the authors of the study conducted an in-depth thermodynamic analysis, maintaining that surface concentrations of the reactants and products, as well as the stabilizing effect of additional H_2O molecules, enable the proposed reaction. Such ongoing debate is evidence that the mechanisms of metal oxide redox are often poorly understood; hence, we will benefit from theoretical guidance in our design and synthesis of oxygen carriers.

In addition to CH_4, CLSO has also been applied to the direct conversion of other light alkanes and olefins. Around 2000, Grasselli used metal oxides such as Bi_2O_3 and In_2O_3 for selective H_2 combustion to improve the Pt-catalysed dehydrogenation of light paraffins in reactors operating in co-feeding and redox modes[69,70]. Supported VO_x materials have been widely studied for oxidative dehydrogenations, including in the so-called riser–regenerator redox system[71,72]. A series of Fe-based and Mn-based redox catalysts for the chemical looping oxidative dehydrogenation of C_2H_6 afforded C_2H_4 in high yield and selectivity (90%)[73–77]. The C_2H_4 product itself can also participate in a further loop involving its epoxidation mediated by an Ag catalyst and a $SrFeO_3$ material as an oxygen carrier[78]. These CLSO success stories provide much hope for the sustainable utilization of hydrocarbon feedstocks, especially for producing valuable chemicals from inexpensive and abundant shale gas supplies. The technologies described here are representative of the historical development of CLC, CLPO and CLSO technologies (FIG. 2) and reflect the importance of oxygen carriers.

The slow initial pace at which chemical looping processes developed was mainly a result of rapid deactivation of the solid carriers at high temperatures. This was compounded by the high costs of scaling up and constructing related reactors and the trial-and-error nature by which oxygen carriers were screened. Recent advancements in catalysis science and chemical engineering have enabled chemical looping processes for the clean and efficient production of power, fuels and chemicals. The efficiency of these modern processes rests on the oxygen carriers having a number of desirable characteristics. These carriers must be chemically and physically stable, economically viable and environmentally benign. Moreover, their reactions must be thermodynamically and kinetically favourable and be highly selective for the desired products. The following sections describe the functions of oxygen carriers and recent means by which we can improve their performance.

Oxygen carrier functions

Oxygen carriers are typically porous solids with high surface areas and low transport resistances between the external atmosphere, intraparticle pores and particle surface. Oxygen carrier particles consist of reducible MO_x compounds with three key functions: generating oxygen ions or vacancies and electrons or holes, facilitating their diffusion in the bulk phase and providing active sites for surface reactions (FIG. 3). We now consider the reduction step — the step in which the carrier is reduced and the reactant is oxidized. Here, the oxygen-rich carrier particles can absorb thermal energy and generate active oxygen species at high temperatures. When the particles are exposed to reducing gases, oxygen anions permeate from the bulk to the surface because of an oxygen chemical potential gradient, which is balanced by a countercurrent flow of electrons to maintain the overall charge neutrality. On the particle surface, oxygenic species react with reducing agents at specific active sites to form the desired products. During the oxidation step (reduction of the reactant gas), surface exchange and reaction occur with the generated oxygen ions and electron holes, which subsequently diffuse inward and combine with oxygen vacancies in the bulk.

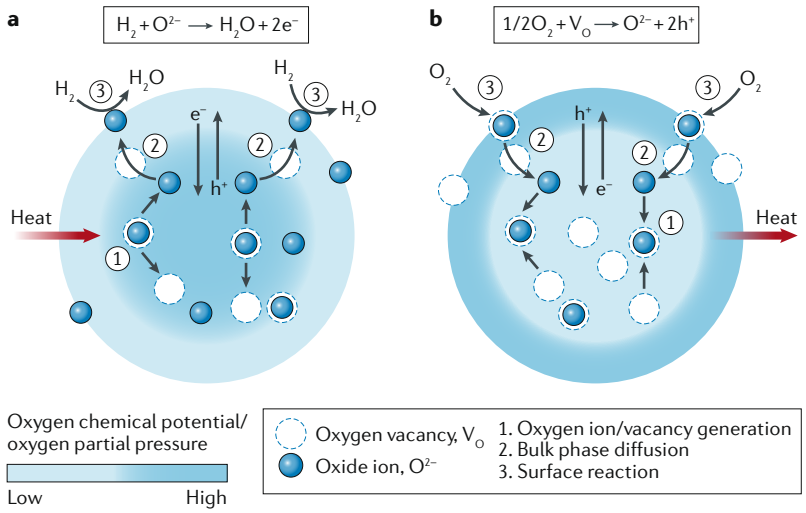

Fig. 3 | **An oxygen carrier particle can be reduced by H_2 and reoxidized by O_2.** **a** | Exposing a metal oxide particle to H_2 removes a surface O^{2-} ligand as H_2O, triggering migration of more O^{2-} to the surface, with local charge being balanced by the movement of electrons to the centre of the particle. **b** | When the material contacts O_2, electrons move to the surface, yielding O^{2-} ligands that fill the oxygen vacancy (V_O)[6,61,77].

Oxygen carriers necessarily feature reducible metal oxides, prominent examples of which are Fe_2O_3 and CuO. These active materials are often complemented by dopants, supports (for example, Al_2O_3) or other structures that improve their function[55,79–81]. The generation and storage of oxygen ions and vacancies hinges on the thermodynamic oxygen potential of the metal oxides, which is the most important factor governing whether or not CLFO or CLPO can proceed. The thermodynamic properties can be affected by the presence of dopants, and these modified materials may undergo redox reactions at low temperatures. Once oxygen anions or vacancies are formed, we must be concerned with their bulk phase ionic diffusion, which determines the rate of release and replenishment of lattice oxygen. Certain crystal structures are more amenable to fast diffusion, something that can also be influenced by bulk doping. Once at the surface, the oxygen anions or vacancies combine more effectively with reactants when they are at specific catalytic sites. Furthermore, when oxygen carriers are used in CLSO, it is important to control the distribution of the oxygen supply in the bulk as well as the types of active oxygen species (for example, O^{2-}, O^- and O_2^-) at the surface. This is necessary to achieve high reactant conversions and product selectivities.

For practical applications, oxygen carriers in chemical looping processes must meet a number of criteria. They must exhibit long-term redox stability, existing in only the two (or more) states relevant to the reactions in the loop. The carriers should also have fast reaction kinetics, possess favourable thermodynamics, exhibit reasonable oxygen and heat capacity and conductivity, be mechanically and thermally robust under the operation conditions and have a low monetary cost. The reactions with oxygen carriers involve the generation and transfer of different oxygenic species in the bulk phase and can afford different products depending on the specific surface reaction pathway. For example, we noted above that reactions with alkane feedstocks may afford fully oxidized products (H_2O/CO_2), partially oxidized products (H_2/CO) or even less-oxidized species such as olefins and higher hydrocarbons. These oxidations often have complex mechanisms and branching pathways, with the presence of non-equivalent surface sites further complicating product distribution. This scenario has inspired many studies focused on understanding mechanisms and controlling kinetics and selectivity. We now describe the thermodynamics and crystal structures of metal oxides, followed by the important factors governing bulk phase diffusion and surface reaction mechanisms.

Metal oxide redox thermodynamics

We consider metal oxides in the context of oxidizing a carbonaceous feedstock to CO_2/H_2O (CLFO) and/or CO/H_2 (CLPO). The thermodynamic properties of oxides dictate their suitability for the reactions and the resulting product selectivity. In particular, metal oxides can be studied and categorized on the basis of their equilibrium oxygen potential, which is best illustrated in a modified Ellingham diagram[7,82] (FIG. 4a). If we also plot the equilibrium oxygen partial pressures (p_{O_2}) associated with the full and/or partial oxidation of feedstocks such as CH_4, C, CO and H_2, we get an idea of which oxides are useful for CLFO and which ones are more useful for CLPO. For CLFO, an oxide should have an equilibrium p_{O_2} above the lines for CO and H_2 combustion. Thus, the Mn, Fe and Cu oxides, whose curves are located in the upper CLFO region, can mediate conversions into CO_2 and H_2O. The strongest oxidants — Mn_2O_3, Co_3O_4 and CuO — release O_2 even at moderate temperatures[83]. By contrast, the equilibrium p_{O_2} values for $CaSO_4$, NiO and CoO lie near the bottom of this CLFO region, closer to the CO and H_2 combustion curves, such that some of these fuels may remain unreacted if inside a reducer bearing these metal compounds. In general, the oxygen carriers in this CLFO group are primarily studied either for CLC with CO_2 capture or O_2 generation related to CLOU or air separations. Below the CLFO region but above the line of CO formation is the CLPO region, in which lie p_{O_2} curves for metal oxides that are thermodynamically competent for gasifying C to CO but not oxidizing it (or H_2) any further. Metal oxides in this region can be used for syngas production from feedstocks such as coal and natural gas. In principle, one could alternatively make syngas from hydrocarbons over a metal oxide in the CLFO group, as long as it is present in a substoichiometric (available lattice O atoms:fuel) ratio, but the resulting syngas concentration is highly dependent on the oxygen:fuel ratio. The advantage of using metal oxides in the CLPO group is that they can thermodynamically ensure the stable production of high-purity syngas while minimizing C deposition[16]. A small subgroup of metal oxides — including FeO, Fe_3O_4, WO_2 and MoO_2 — are suitable for thermochemical H_2O and CO_2 splitting (FIG. 4a, right panel). These oxides are in the vicinity of the line for CO/H_2 combustion; thus, it is thermodynamically feasible that they can be reduced by a CO-rich or H_2-rich stream and reoxidized by a CO_2-rich or H_2O-rich stream as part of an overall chemical looping reforming process or reductions of CO_2 or H_2O. A third group of metal

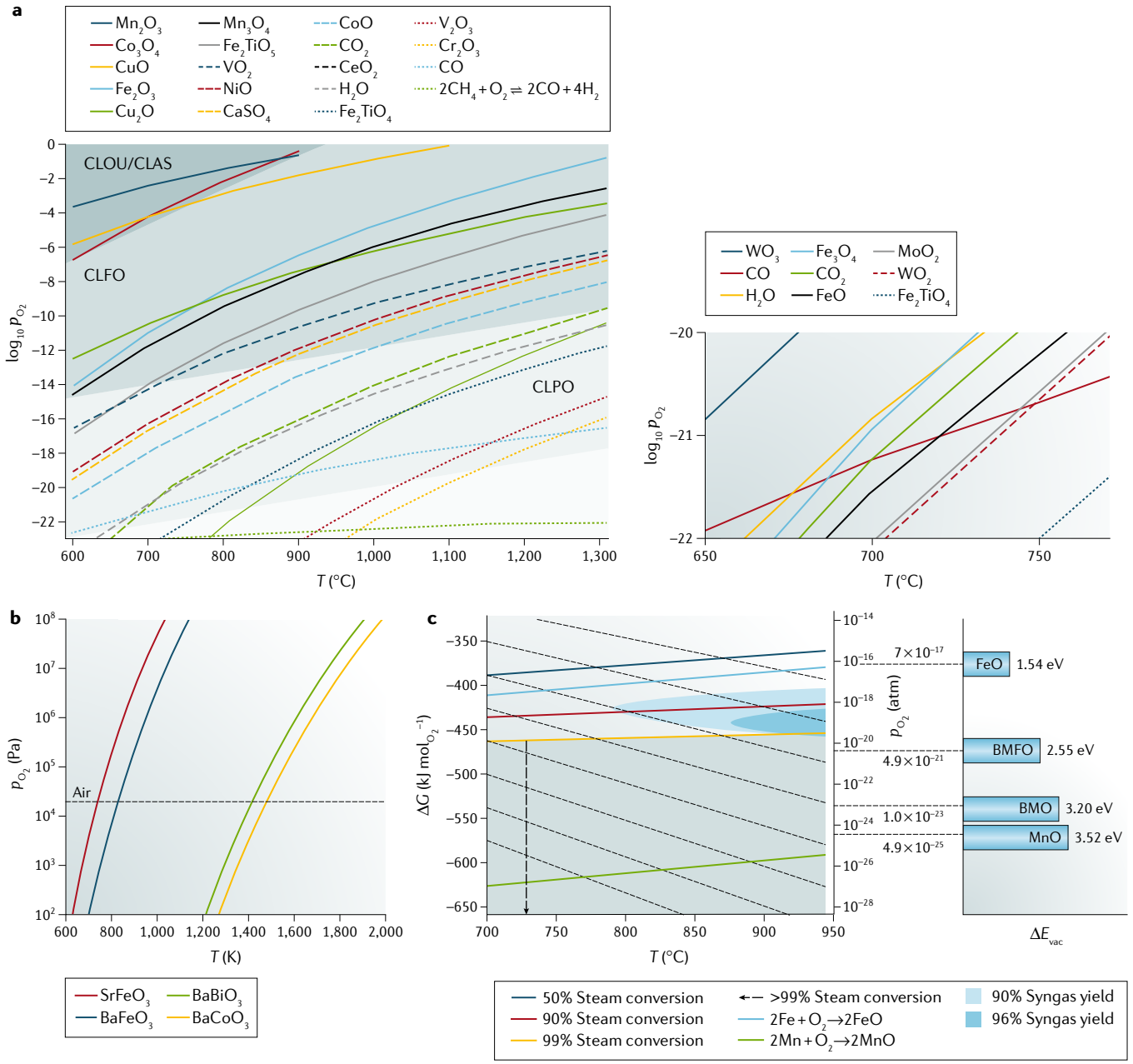

Fig. 4 | **Modified Ellingham diagrams for unary, binary and ternary metal oxides, as well as typical feedstocks.** **a** | Unary metal oxides with high equilibrium partial O_2 pressure (p_{O_2}) values are strongly oxidizing and can mediate full oxidation of H_2 or C/CO. Oxides with intermediate p_{O_2} values are better suited for partial oxidations (blue region)[82]. A subgroup of oxides is useful for chemical looping reforming or H_2O/CO_2 splitting (right panel). Oxides with lower p_{O_2} curves are inactive. **b** | Binary oxides of the form ABO_3 (perovskites) can lose O_2 at mild temperatures and can be employed in chemical looping for air separation[84]. **c** | The doped perovskite $BaMn_xFe_{1-x}O_{3-\delta}$ has oxidation properties in between FeO and MnO, making it ideal for chemical looping reforming[52]. In this process, CH_4 is partially oxidized to $CO + 2H_2$ on the illuminated perovskite. The reduced perovskite is then reoxidized with H_2O to afford more H_2 and complete the loop. ΔE_{vac}, energy required to form an oxygen vacancy; ΔG, change in Gibbs free energy; CLAS, chemical looping with air separation; CLFO, chemical looping with full oxidation; CLOU, chemical looping with oxygen uncoupling; CLPO, chemical looping partial oxidation; *T*, temperature. Part **a** is adapted with permission from REF.[82], Wiley-VCH. Part **b** is adapted with permission from REF.[84], RSC. Part **c** is adapted with permission from REF.[52], Wiley-VCH.

oxides have p_{O_2} curves at the bottom of the Ellingham diagram. These oxides have little or no oxidation activity, although they may still find use as support materials or dopants as part of active oxygen carrier materials.

Studies on monometallic oxide carriers have recently been extended by research directed towards using materials featuring multiple metals as improved carriers (FIG. 4b). Again, the goal is to discover novel binary or ternary metal oxide materials with an oxygen potential suitable for chemical looping. Robustness is also important, and on this front, an Al_2O_3-supported composite oxygen carrier, which converts between $FeTiO_3$ and Fe_2O_3/TiO_2

forms, has recently been shown to exhibit high activity and recyclability over 3,000 redox cycles at 1,000 °C (REF.[59]). Combinations of Fe and Ti oxides have desirable thermodynamic properties that are essential for the generation of high-quality syngas from shale gas[16]. These properties are complemented by the stability afforded by the Al-based support, which affords composites that have extremely low attrition indices (0.05–0.1 wt%) after extensive testing in pilot-scale and sub-pilot-scale reactors. Such results indicate that the use of oxygen carriers featuring multiple metals may accelerate the development of chemical looping technology towards commercial deployment.

The development of computational chemistry methods and high-performance computing systems has improved our capability to discover and screen novel binary and ternary metal oxides for use as oxygen carriers. For example, the in silico screening of bimetallic oxide materials for chemical looping air separation has been achieved using the Materials Project database to calculate Gibbs free energies at 0 K, and one can then use open phase diagrams to predict equilibrium p_{O_2} values at various temperatures[84] (FIG. 4b). Candidate materials such as $SrFeO_3$ can vary between perovskite and brownmillerite forms, and these show favourable theoretical redox equilibria and resistance to carbonation at low temperatures. Moving to ternary oxides, the perovskite $BaMn_xFe_{1-x}O_{3-\delta}$ mediates efficient conversion of CH_4 and H_2O to give syngas and H_2 in 90% selectivity over two separate steps[52]. In the reducer, the perovskite mediates solar-driven partial oxidation of CH_4 to CO and $2H_2$. The resulting reduced perovskite is then moved to the oxidizer, in which it is reoxidized by H_2O with the concomitant formation of H_2. The perovskite and other oxides can also be studied using density functional theory (DFT) calculations and Ellingham diagrams, affording thermodynamic properties including p_{O_2} values and the energy required to form oxygen vacancies (ΔE_{vac}; FIG. 4c). The ΔE_{vac} value for the perovskite is between those of FeO and MnO, and the perovskite has properties that make it useful for both steam conversion and syngas formation. Such materials may still be improved upon, something that might occur through the systematic screening of more complex systems, including quaternary phases, doped perovskites and non-stoichiometric intermediates. These studies would aim to more accurately model the reaction pathways to identify the design principles for effective oxygen carriers.

Crystal structures and oxygen vacancies

When inside a reducer, oxygen carriers donate O atoms to a fuel and begin to incorporate lattice vacancies into their structures. Such vacancies, either on the surface or in the bulk of a metal oxide, change the geometric and electronic structure of the metal oxide, as well as its chemical properties. A suitable host system should allow for fast transport of lattice O atoms or anions towards the surface, which must maintain its integrity despite sustaining the vacancies formed in the transport process. Once lattice oxygen atoms have migrated to the surface, they can participate in the oxidation of carbonaceous feedstocks. If performing selective oxidations, one must consider many factors, including the bond strength of the surface M–O bonds. If the bonds are too weak, then the O atoms are too easily released and the reactants on the surface may undergo overoxidation. If the bonds are too strong, then the material is too weak an oxidant[85]. An ideal oxygen carrier has an intermediate bond strength and mobile lattice O atoms such that the material can be selective as well as kinetically fast. To sustain sufficient concentrations of O vacancies, a carrier needs to have an appropriate ΔE_{vac} value such that the requisite number of lattice O atoms can reach the surface. This process occurs smoothly in fluorite, perovskite and rocksalt structures, and it is no accident that most oxygen carriers are based on these motifs.

Fluorite-structured oxides are face-centred cubic species of formula MO_2 and are exemplified by ceria (CeO_2), which has 8-coordinate Ce^{4+} and 4-coordinate O^{2-} (FIG. 5a). CeO_2 is commonly used for oxidation and reduction reactions because Ce can reversibly adopt +III and +IV oxidation states upon the release and binding of O, respectively. Fluorite structures such as CeO_2 have oxygen anion Frenkel defects, where an O^{2-} ligand moves from a lattice position of an interstitial site. Thus, one can generate solid solutions with oxygen vacancies simply by aliovalent substitution — replacing a tetravalent cation ion in the host structure with a less positively charged ion[86]. We note that when M^{4+} ions are too small to be 8-coordinate, they instead adopt the rutile structure, which is observed for oxides such as VO_2, WO_2, MoO_2, CrO_2 and MnO_2.

The 1990s saw the investigation of CeO_2 in the conversion of CH_4 into syngas[53], with the chemical looping being based on CeO_2 donating lattice O atoms for the partial oxidation. Thermodynamically, CH_4 oxidation on CeO_2 has a very high conversion and high selectivity towards CO and H_2 (REF.[7]). Exposing CeO_2 to carbonaceous gaseous fuel at high temperatures results in the removal of lattice O atoms and the formation of several phases of formula CeO_{2-x} ($0 \leq x \leq 0.5$)[87]. Despite the structural properties of CeO_{2-x} being the subject of a variety of spectroscopic studies, there are still difficulties in the experimental determination of vacancy-induced structural relaxations and ΔE_{vac} values. Recent advances in computational techniques have largely overcome these hurdles. The structural changes induced by the introduction of O vacancy formation on CeO_2 can be characterized using DFT calculations with the spin-polarized PW91 functional for the open-shell species CeO_{2-x}. Ce centres adjacent to oxygen vacancies were predicted to move away from the defect while the nearest lattice oxygen atoms contract towards the vacancy[88]. Another DFT study considered the electronic structure of oxygen vacancy defects at the low index surfaces of CeO_2 and showed that although the thermodynamic stability of the surfaces follows the order (111)>(110)>(100), it is the (110) surface that has the lowest vacancy formation energy[89]. Thus, the metastable CeO_2(110) surface would be the most active for redox reactions. A detailed DFT investigation into oxygen vacancies on CeO_{2-x}(110), involving correction of the on-site Coulomb correlation through a Hubbard U-term, revealed two distinct types of sites: in-plane vacancies and split vacancies (FIG. 5a).

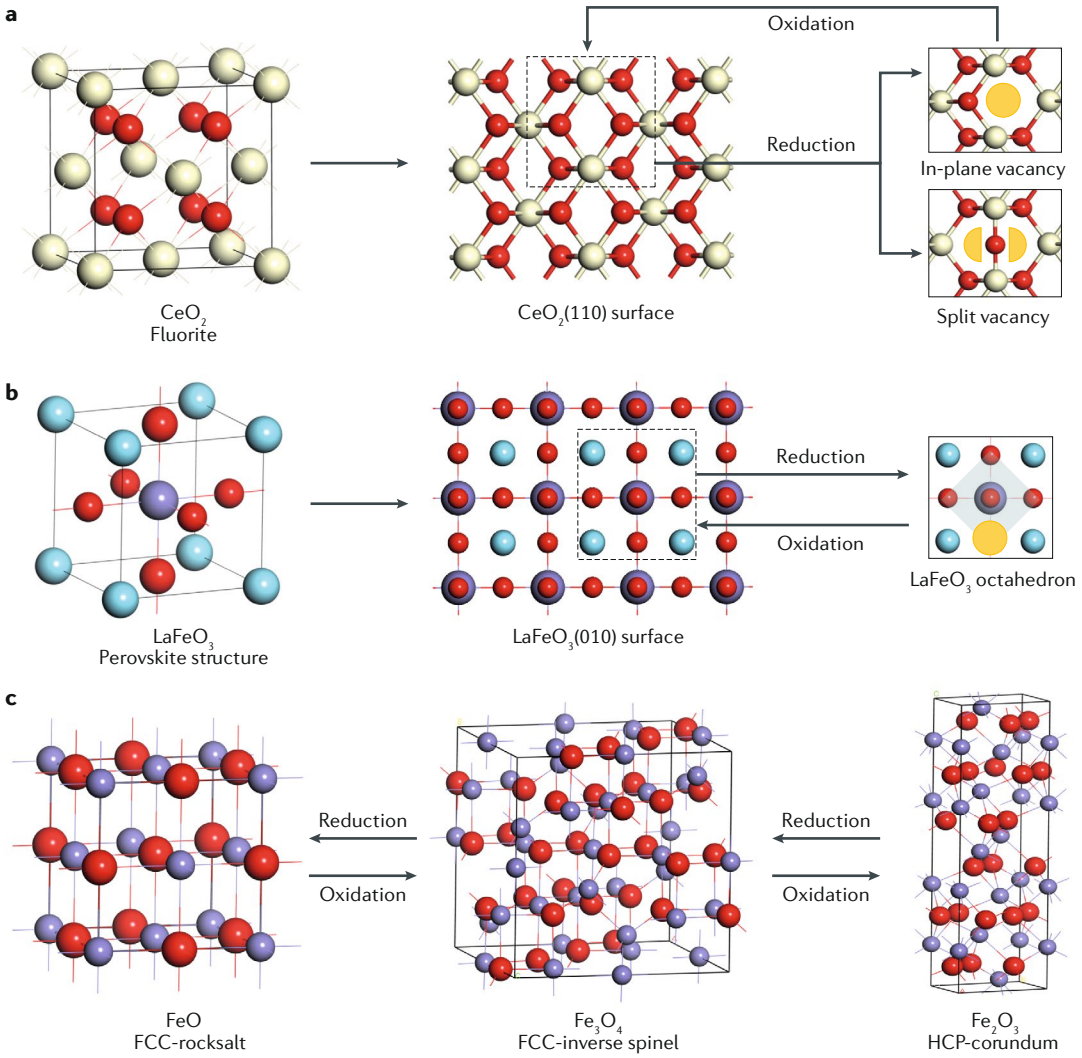

Fig. 5 | **Representative crystal structures of metal oxide oxygen carriers. a** | CeO_2 adopts a fluorite structure, and its (110) surface can undergo reduction to afford an in-plane or split O vacancy[90]. **b** | $LaFeO_3$ assumes a perovskite structure, of which the (010) surface is the most reactive in redox processes[145]. **c** | Fe is very redox-active, and the reduced FeO form can be converted into Fe_3O_4 and Fe_2O_3. Part **a** is adapted with permission from REF.[90], AIP Publishing.

The formation of a split vacancy (ΔE_{vac} = +1.651 eV) is more favourable than an in-plane vacancy structure (ΔE_{vac} = +1.962 eV)[90], indicating that structural relaxation can substantially affect oxygen vacancy formation energies. Theoretical calculations have also shown that the ΔE_{vac} values, which are related to the reducibility of a metal oxide, are approximately 30% lower for CeO_2 surfaces relative to the bulk. Thus, the surfaces of CeO_2 are not only more accessible to reactants and the bulk but also energetically more amenable to redox reactions involving the exchange of O atoms between adsorbates and CeO_2 (REF.[91]).

The perovskite structure ABO_3 (FIG. 5b) features different cations A^{x+} and $B^{(6-x)+}$, and it is similar to the fluorite structure in that it can accommodate cations with a wide range of charges and ionic radii[92]. A metal oxide perovskite can thus contain a high concentration of oxide vacancies and have high ionic conductivity. For example, the materials $AFeO_3$ (A = La, Nd or Eu), prepared using a sol–gel method, exhibit high activity for the partial oxidation of CH_4. Among the three perovskites, $LaFeO_3$ shows the highest selectivity for syngas (90% at 900 °C), with the CH_4 conversion also being high (65%)[93]. This finding encouraged further studies of $LaFeO_3$ as the active component in oxygen carriers for CH_4 conversion in chemical looping. Other methods exist for preparing $LaFeO_3$, including the evaporation and calcination of an aqueous mixture of $La(NO_3)_3$, $Fe(NO_3)_3$, NH_3 and DL-tartaric acid[94]. The product has high surface area and reactivity, and these can be further improved by aliovalent substitution[95], which introduces more oxygen vacancies. The redox processes at the (010) facet of $LaFeO_3$ include reduction, whereby oxygen vacancies form, and healing, which involves reoxidation (FIG. 5b). The O content in perovskites can be variable such that one can have solid solutions of the form $ABO_{3-\delta}$, in which oxygen vacancies are randomly distributed. For example, brownmillerite oxides of formula $A_2B_2O_5$ can be considered O-deficient perovskites, and these exhibit fast ionic diffusion along 1D pathways in

(010) planes[84]. It is difficult to determine what structures should be considered as distinct phases because small changes in composition can lead to different defect arrangements; thus, a comprehensive understanding of vacancy formation and ion migration is needed.

Fe oxides have been extensively studied as oxygen carriers for the CLPO of CH_4 to syngas[1,14]. In this process, adsorbed CH_x species accept oxygen atoms, leading to the formation of oxygen vacancies. Reactions between Fe oxides and CH_4 are complicated because of the stepwise reduction to Fe_2O_3 and then to Fe_3O_4 and FeO (and possibly also to Fe)[96,97]. The oxides Fe_2O_3, Fe_3O_4 and FeO have similar close-packed arrangements of O atoms (FIG. 5c), and each can thus have similar oxygen vacancies[98,99]. The CLPO process can be modelled by considering the case of CH_4 adsorption on Fe_2O_3, Fe_3O_4 and FeO surfaces, and calculations show that surface oxygen vacancies can facilitate CH_4 oxidation by lowering the activation barriers to the formation of CH_3, CH_2 and CH species[100]. The ΔE_{vac} value for $FeTiO_3$ is approximately 0.5 eV lower than that for Fe_2O_3. $FeTiO_3$ has a hexagonal close-packed structure, with the metal ions occupying two-thirds of the available octahedral sites. Lattice oxygen atoms are octahedrally coordinated to the Fe^{2+} and Ti^{4+} ions, with the edges of the octahedra being the most favourable sites for oxygen vacancies[62]. To summarize, the oxidation states, ionic radii, coordination requirements and bonding energies of metal ions and O^{2-} ligands are strongly dependent on the crystal structure. Thus, it is the structure that dictates how readily oxygen vacancies can form. An understanding of the various crystal structures and oxygen vacancies is helpful in predicting bulk ion transport and surface reactions of metal oxides, topics we now outline.

Ionic diffusion and morphological evolution

Although thermodynamic analysis can assist in identifying potential oxygen carriers, we then need to prepare the materials and subject them to systematic physical and chemical characterization before evaluating their performance in terms of redox kinetics and stability. The reactivity of oxygen carriers plays a key role in determining how effectively they process carbonaceous fuels, the product distribution and the overall chemical looping process efficiency. As mentioned above, the reduction of solid carriers involves the donation of O atoms to effect the full, partial or selective oxidation of carbonaceous feedstock. In the oxidation step, the depleted oxygen carriers are replenished with O_2 from air in an exergonic reaction. Alternatively, the oxidation step can also be triggered by exposure to CO_2/H_2O, which can donate O atoms to regenerate the oxide and release CO/H_2. The stepwise stoichiometric reactions of solid oxides in chemical looping are fundamentally different from heterogeneous catalysis, as the former involves substantial changes in the morphology of the oxides due to the ionic diffusion, oxygen vacancy formation and migration both in the bulk and on the surface. Therefore, an understanding of the underlying solid state chemistry is essential to the design and development of robust oxygen carriers that exhibit high reactivity.

Ionic diffusion is an important fundamental factor in determining the rates at which reactions of metal oxides occur. As with diffusion in the gas or liquid phase, diffusion in solids is entropically driven by a concentration (chemical potential) gradient, with ions moving from a region of high concentration to a region of low concentration. In structures with cubic close-packing of the oxygen ions (for example, spinel structures), vacancies in the oxygen sublattice have higher formation enthalpies than do defects in the cation sublattice. Lattice oxygen defects are thus present at lower concentrations, and the diffusion of lattice oxygen is correspondingly slower than the diffusion of cations. By contrast, in oxides with more open oxygen sublattices (for example, perovskite structures), oxygen vacancies are more energetically accessible than cation defects. Consequently, these oxides show high lattice oxygen diffusivities and can function as good oxygen carriers for chemical looping processes.

One means to study diffusion in oxides is to use isotopic labelling, and the radioactive tracer ^{18}O has been used for decades in experimental studies, including in classic investigations of ionic diffusion in $CaSO_4$ (REFS[101,102]). This method has been applied to a single-crystalline $MgO{\bullet}nAl_2O_3$ to show that the activation energy of lattice oxygen self-diffusion (exchange) is 439 kJ mol^{-1} (REF.[103]). This value is only very slightly (~4 kJ mol^{-1}) higher for $MgAl_2O_4$ on an Al_2O_3 support, implying that the concentration of the mediating O vacancy is unaffected by the incorporation of Al^{3+}. However, the use of polycrystalline $MgO{\bullet}nAl_2O_3$ affords an activation energy of 384 kJ mol^{-1}, suggesting that grain boundaries have an important effect on diffusion[104]. By conducting depth profiling experiments on the metal oxide, Reddy and Cooper obtained oxygen diffusion barriers of ~370 kJ mol^{-1} for MgO and ~405 kJ mol^{-1} for Fe_2O_3 (REF.[105]). Recent years have seen studies of diffusion by computer simulations, and the atomistic temperature-accelerated dynamics technique has enabled the prediction of diffusion energies for the intrinsic defect processes capable of facilitating lattice O diffusion in $MgAl_2O_4$, $MgGa_2O_4$ and $MgIn_2O_4$ (REF.[106]). This study showed that the activation energy for the interstitial diffusion of lattice oxygen is lower than that for vacancy-mediated diffusion. These simulations of ionic diffusion were soon complemented by DFT calculations, which became commonplace in chemical looping processes during the late 2000s[107,108]. The calculations involve setting up the atoms in an initial state with possible interstitial sites through which the ions of interest can diffuse. Once all the likely diffusion pathways are identified, it is possible to calculate the total system energies corresponding to the different locations of the ions on the pathway. The diffusion energy barrier is defined as the energy difference between the highest energy state on the pathway and the energy of the initial state. By calculating the diffusion energy barriers, one can determine the diffusivities of different ions and find the most favourable diffusion pathways.

As we alluded to in the discussion regarding single-crystalline and polycrystalline $MgO{\bullet}nAl_2O_3$, morphology can greatly affect ionic diffusion, which in

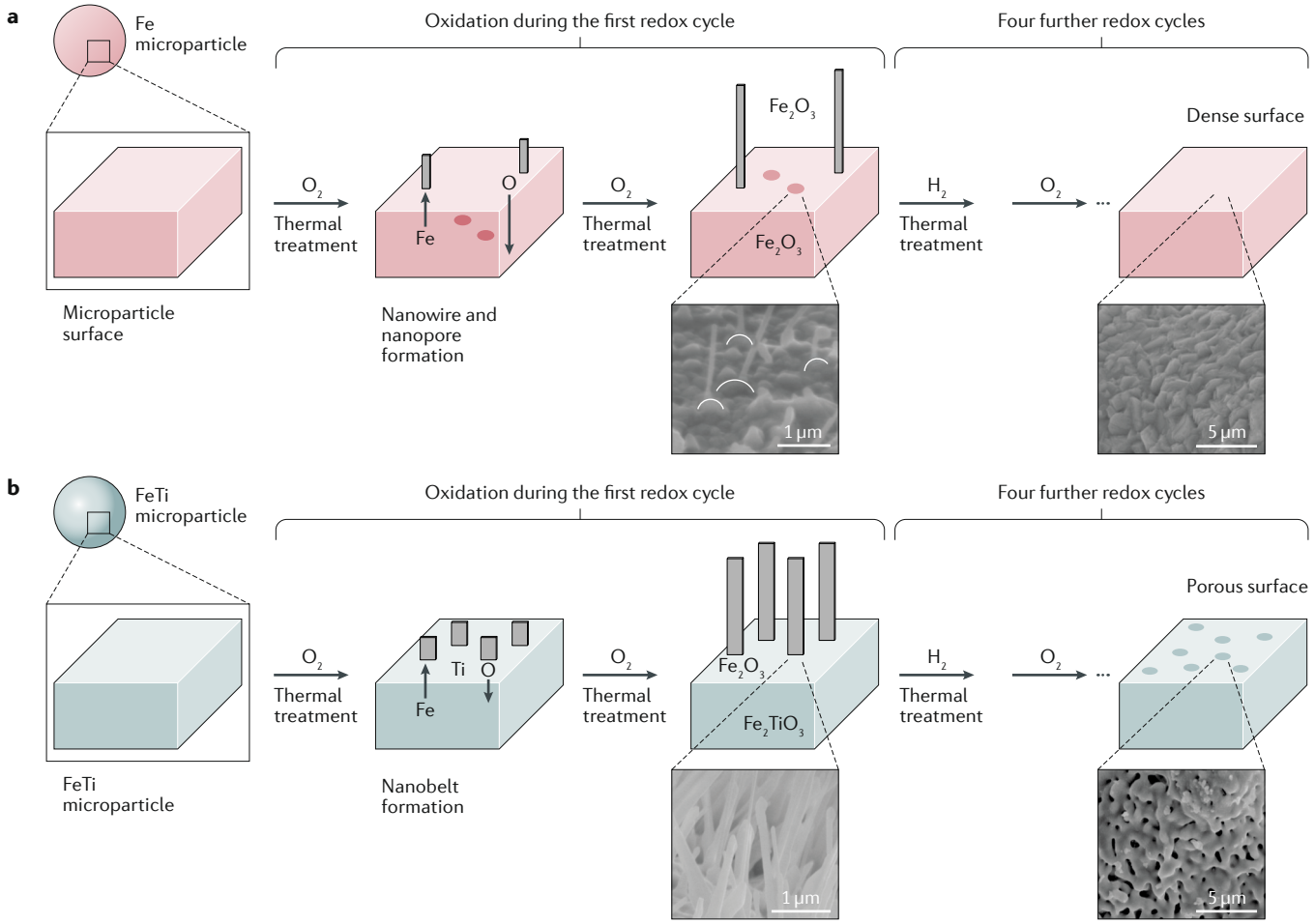

Fig. 6 | **The morphological evolution of metal microparticles during chemical looping. a** | The oxidation of Fe results in Fe migration to the surface, leading to the formation of nanowires and nanopores[110]. **b** | In the case of FeTi, the Fe centres again migrate to the surface, while the more highly charged Ti ions do not move. Insets show scanning electron micrographs of the Fe and FeTi systems after one and five redox cycles[62]. Part **a** is adapted with permission from REF.[110], RSC. Part **b** is adapted with permission from REF.[62], RSC.

turn affects active-site availability. It is thus important to understand the morphological evolution of a metal oxide under redox conditions. For the Fe oxide system, a concentration gradient exists throughout the particle during the oxidation process, causing Fe ions to continuously diffuse from the core to the surface, thereby leaving a porous centre[109] (FIG. 6a). At 700 °C, Fe_2O_3 exhibits greater outward Fe diffusivity than inward O diffusivity, such that net Fe diffusion occurs from the centre to the edges[110]. This outward Fe diffusion is further enhanced because the high volume expansion of Fe to Fe_2O_3 creates physical space through which the Fe ions can migrate. The net flux of Fe is balanced by an opposite flux of O vacancies, which can condense into pores at dislocations. The stress-driven expansion and curvature-driven grain growth trigger the formation of nanowires and nanopores, which are readily evident in scanning electron micrographs.

As with the oxidation of Fe, the oxidation of binary FeNi microparticles converts a non-porous material into one having a porous centre. The introduction of porosity and volume expansion are accompanied by fast migration of Fe and slow migration of Ni towards the surface, affording a structure with an Fe-oxide-rich shell and a Ni-oxide-rich core. The former component consists of nanopores and nanowires, much like the surface of oxidized pure Fe microparticles[110]. Although CuNi is similar in that it develops porosity upon oxidation, it does not form the core–shell structure or develop nanostructures during the redox process. We have already noted the prominence of $FeTiO_3$ as an oxygen carrier; hence, it seems important to also consider the oxidation of FeTi microparticles. These behave differently to FeNi or CuNi microparticles because Fe is the only active component, while Ti acts as an inert support material. The oxidation of FeTi produces $FeTiO_3$ particles with nanobelts on the surface[62]. The nanobelts have widths of 150–200 nm and width:thickness ratios of 5–10, and they protrude from the surface and mainly contain Fe and O (REFS[111–113]) (FIG. 6b). Reduction of the oxidized microparticles causes the nanobelts to partially retract, leading to increased porosity throughout the particle, which now has a uniform elemental distribution. The porosity of $FeTiO_3$ microparticles after five redox cycles is greater than the porosity after one cycle, suggesting that the inclusion of Ti as a support confers recyclability on the Fe system

while maintaining reactivity. The excellent reversibility of this redox system is evident by its persistent reactivity over 1,000 redox cycles[1,59]. The scanning electron microscopy of the redox processes is complemented by atomistic thermodynamics methods and DFT calculations on $FeTiO_3$. These studies predicted a higher diffusivity for Fe^{2+} at 1,173 K ($2.21 \times 10^{-7}\ m^2\ s^{-1}$) relative to that for Ti^{4+} ($1.35 \times 10^{-10}\ m^2\ s^{-1}$). Perhaps a result of its lower ionic charge, Fe^{2+} undergoes faster outward diffusion than does Ti^{4+}, which explains the formation of the Fe_2O_3 nanobelts and the superior recyclability of FeTi microparticles over that of pure Fe microparticles[62].

Surface reactions and modifications

Metal oxide materials can be useful oxygen carriers for chemical looping applications, including in the partial oxidation or oxidative coupling of CH_4, CO oxidation and CO_2 reforming. Thus far, we have described how metal and oxygen ions move throughout particles, noting the importance of understanding how oxygen vacancies form and lattice oxygen diffuses. This knowledge provides theoretical guidance for the sustainable synthesis of oxygen carriers for chemical looping and also allows us to not only rationalize their performance but also predict it in advance, such that a minimum amount of trial-and-error screening is required. This rational development of oxygen carriers must consider not only the movement of ions throughout particles but also the mechanism by which reactants are processed on the oxide surface. The following section is devoted to this concept.

We introduce our discussion on surface reaction pathways by taking the important example of generating syngas, a versatile product that is commonly made by partial oxidation of carbonaceous fuels through either gasification or reforming[14]. These CLPO reactions have been studied using Mn, Co, Ni, Cu and Fe oxides, with the latter being the most attractive oxygen carriers owing to their cost:benefit ratio and high versatility[114–119]. Indeed, Fe-based oxygen carriers can afford syngas at a concentration higher than 90% with full fuel conversion[16], promoting the study of the mechanisms by which these carriers operate. Towards this, the reduction of Fe_2O_3 and evolution of gaseous products during CH_4 oxidation can be studied under different reaction atmospheres using thermogravimetric analysis coupled with mass spectrometry. For example, this process was applied to the oxidation of dilute CH_4 in air (ventilation air methane from coal mines), and the presence of O_2 did not allow Fe_2O_3 and CuO to undergo reduction during looping[120]. Teasing out mechanistic details through experimentation alone has proved difficult owing to limitations in detecting CH_x fragments and intermediates. Complementary ab initio DFT+U calculations on the partial oxidation of CH_4 to syngas over an Fe oxide oxygen carrier[121] revealed that CH_4 adsorbs onto surface Fe sites and is cleaved to afford CH_3, CH_2, CH and then C at surface oxygen vacancies. The hydrogen ions released are adsorbed at the Fe sites and then undergo reductive coupling to form H_2. Meanwhile, subsurface O atoms diffuse to the vacancy sites, forming bonds with the adsorbed C radicals to give CO. An increase in the concentration of oxygen vacancies facilitates CH_4 partial oxidation by lowering the activation barriers for C–H and Fe–C bond cleavage. However, increasing the surface O vacancy concentration beyond ~2.5% does not lower the overall activation barrier because it leads to an increase in the barrier-to-lattice oxygen diffusion. Therefore, under a CH_4-rich atmosphere, the availability of O vacancies on Fe oxides favours partial oxidation, while a CH_4-lean stream would instead undergo complete oxidation. These favourable properties of Fe oxides make them ideal for incorporation into composite O atom carriers such as Fe_2O_3@$La_{0.8}Sr_{0.2}FeO_{3-\delta}$ core–shell microparticles, which are active for syngas formation[122]. CH_4 oxidation can occur in four regimes depending on the oxidation states of the metals: unselective oxidation to CO_2 and H_2O; intermediate between unselective and selective; selective oxidation to syngas; and a coking region. The high selectivity towards the formation of syngas in the third regime is attributed to the surface being more depleted in O relative to the surface in the first two regimes. A transient pulse study on this system concluded that the CH_4 oxidation mechanism was not of the Eley–Rideal type (one surface species reacting with a gaseous species) but rather similar to a Langmuir–Hinshelwood mechanism (two surface species reacting with each other)[123]. Overall, it is the surface oxygen vacancy concentration that determines the mechanism of CH_4 oxidation, and we cannot overstate the influence of lattice oxygen diffusion and oxygen vacancies on the mechanisms of reactions in chemical looping.

Recent discoveries of shale gas deposits have motivated us to develop efficient chemical looping schemes for direct CH_4 conversion into not only syngas but also other value-added chemicals[124]. One of the more promising technologies is the OCM, whereby CH_4 is directly converted into C2 hydrocarbons C_2H_6 and C_2H_4. Compared with conventional OCM technologies, chemical looping OCM avoids direct contact between O_2 and CH_4, thereby eliminating the need for an air separation unit and eliminating the hazards associated with flammable CH_4/O_2 mixtures[14,125]. The metal oxides in chemical looping OCM, unlike irreducible catalysts, donate lattice O atoms to CH_4 such that the metal oxides undergo changes in oxidation state and incorporate surface defects. These defects facilitate CH_4 activation by charge transfer[126–128], and there is a correlation between surface charges and C2 product yields. Metal oxides with low bandgaps, such as Mn oxides, exhibit superior performance in the OCM[129,130]. However, there remains uncertainty regarding the origin of selectivity in the OCM[131,132], and this problem is non-trivial because the overall reaction network comprises a series of parallel and consecutive reactions occurring at both the oxygen carrier surface and the gas phase. It is generally accepted that CH_4 first dissociates into CH_3 and H, with two CH_3 groups coupling to form C_2H_6. Subsequently, C_2H_6 undergoes homogeneous or heterogeneous dehydrogenation to give C_2H_4. At a given CH_4 conversion, the product distribution is largely independent of the metal oxide used, indicating that C2 product formation is likely a gas-phase process rather than one occurring on the metal oxide surface.

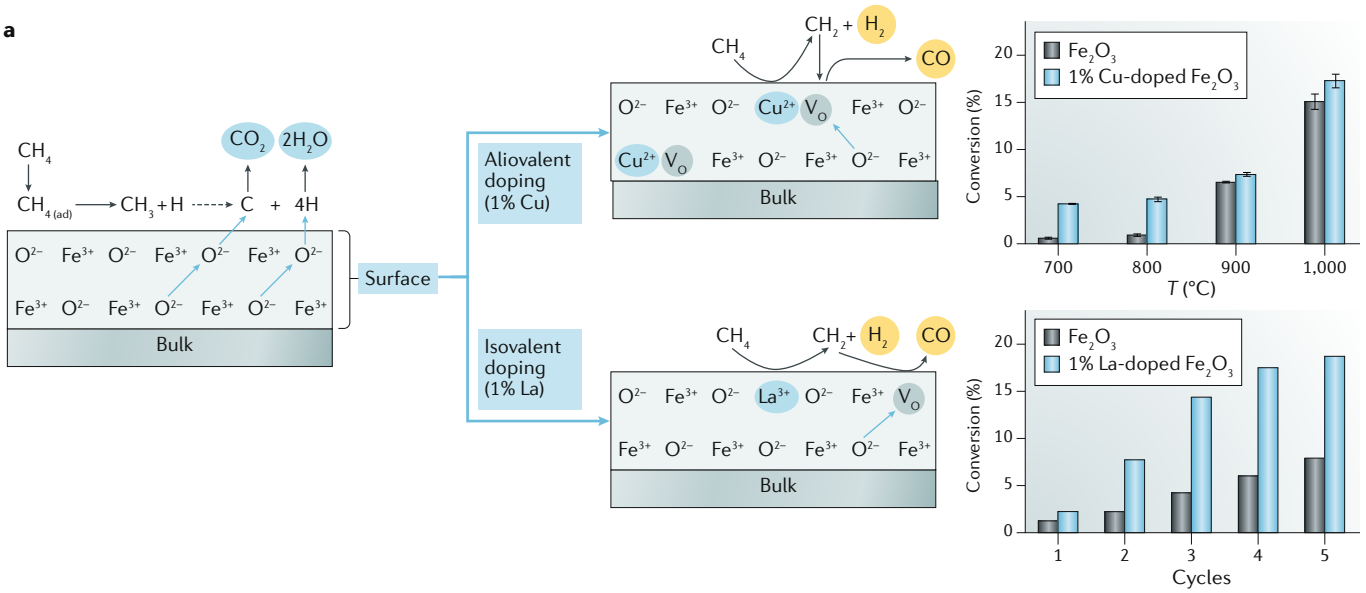
a
CH4
CH4 (ad)
CH3 + H
C + 4H
CO2
2H2O
Surface
Bulk
Aliovalent doping (1% Cu)
Isovalent doping (1% La)
CH4
CH2 + H2
CO
Cu2+ VO
La3+
Fe2O3
1% Cu-doped Fe2O3
1% La-doped Fe2O3
Conversion (%)
T (°C)
Cycles

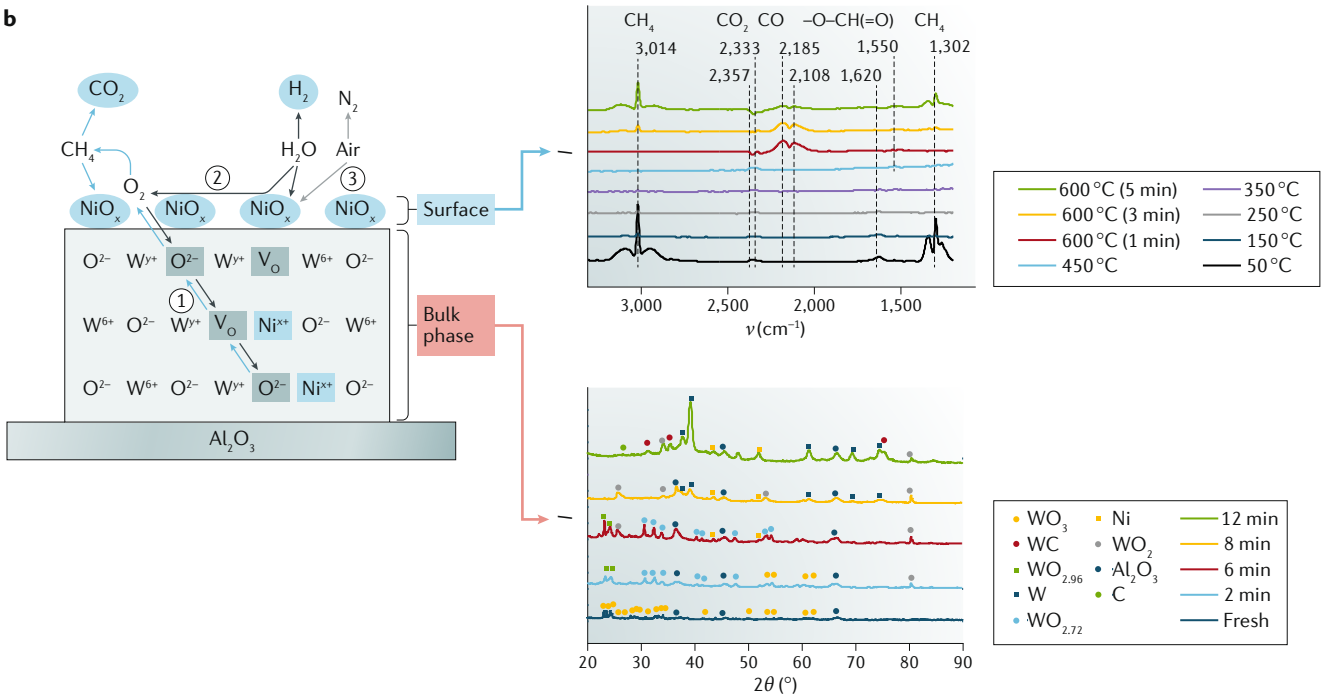
b
CO2
H2
N2
CH4
H2O
Air
O2
NiOx
Surface
Bulk phase
Al2O3
CH4
CO2
CO
–O–CH(=O)
3,014
2,333
2,185
1,550
1,302
2,357
2,108
1,620
ν (cm−1)
600 °C (5 min)
600 °C (3 min)
600 °C (1 min)
450 °C
350 °C
250 °C
150 °C
50 °C
WO3
WC
WO2.96
W
WO2.72
Ni
WO2
Al2O3
C
12 min
8 min
6 min
2 min
Fresh
2θ (°)

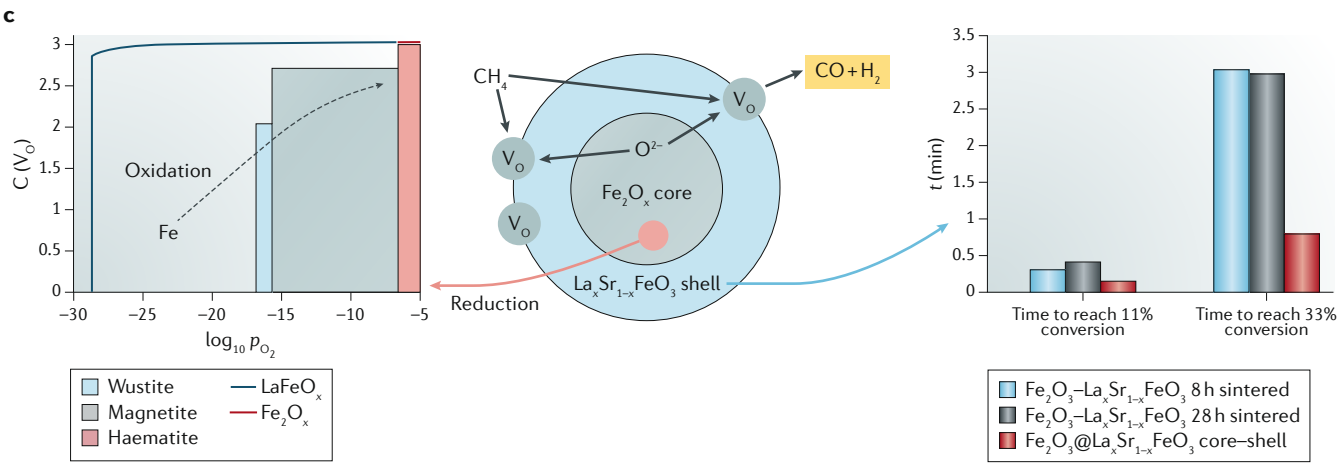
c
C (VO)
Oxidation
Fe
log10 pO2
Wustite
Magnetite
Haematite
LaFeOx
Fe2Ox
CH4
CO + H2
VO
O2−
Fe2Ox core
LaxSr1–xFeO3 shell
Reduction
t (min)
Time to reach 11% conversion
Time to reach 33% conversion
Fe2O3–LaxSr1–xFeO3 8 h sintered
Fe2O3–LaxSr1–xFeO3 28 h sintered
Fe2O3@LaxSr1–xFeO3 core–shell

Fig. 7 | **Modifying the surface of an oxygen carrier can improve its cyclic redox reactivity. a** | Pure and doped Fe_2O_3 both undergo reduction when exposed to CH_4 but afford different products[143,144]. Fe_2O_3 affords CO_2 at low conversions, while 1% aliovalent (Cu^{2+}) or isovalent (La^{3+}) doping of Fe_2O_3 results in materials that afford CO at high conversions. **b** | The supported mixed oxide system $NiWO_x/Al_2O_3$ is an effective oxygen carrier for the oxidation of CH_4. Exposing the carrier to CH_4 for different periods affords different distributions of solid phases according to ex situ powder X-ray diffraction and in situ infrared diffuse reflectance spectra[17]. **c** | The core–shell material Fe_2O_3@ $La_xSr_{1-x}FeO_3$ mediates partial oxidation of CH_4 to give CO and H_2, with the oxygen vacancy (V_O) moving from the core to the surface of the shell. Thermodynamics enables us to predict how the equilibrium oxygen partial pressure (p_{O_2}) affects the V_O concentrations and phases of $LaFeO_x$ and FeO_x that are present (p_{O_2} is measured in atm)[122]. The core–shell Fe_2O_3@$La_xSr_{1-x}FeO_3$ material is superior to the analogous composite Fe_2O_3–$La_xSr_{1-x}FeO_3$ in terms of its rate of CH_4 conversion[123]. *ν*, wavenumber; *I*, intensity; *T*, temperature; *t*, time. Part **a** is adapted with permission from REF.[143], American Chemical Society, and REF.[144], Elsevier. Part **b** is adapted with permission from REF.[17], American Chemical Society. Part **c** is adapted with permission from REF.[122], American Chemical Society, and REF.[123], Wiley-VCH.

The complexity of the OCM mechanism has led some to utilize alternative stochastic approaches to design oxygen carriers that are more efficient for this conversion. For example, a new hybrid genetic algorithm (tested on the travelling salesman problem) was used for global optimization in the design of optimal OCM metal oxides. This multi-turn design strategy involved screening a combination of six metal components and resulted in the discovery of metal oxides that afford 27.8% C2 yield[133]. In another study, the use of statistical analysis in experiment design enabled the identification of a $Mn/Na_2WO_4/SiO_2$ system with C2 yields of 31–33%[134].

As with other reactions, the OCM can be sensitive to the morphology of the oxygen carrier. One can use both hydrothermal and precipitation methods to prepare $La_2O_2CO_3$ samples of different morphologies, with the rod-shaped samples exhibiting the best OCM activity at low temperatures (420–500 °C)[135]. Doping is also important, with a combined experimental and quantum chemical study of chemical looping OCM over a MgMn composite oxygen carrier highlighting that Li-doping induces oxygen vacancies and substantially improves C2 selectivities by increasing the adsorption energy of CH_3 but also increasing the barriers to C–H cleavage[136]. In general, state-of-the-art metal oxide oxygen carriers achieve C2 selectivities of 50–70% at CH_4 conversions of 35–55%, which correspond to C2 yields of 21–33%. Without a doubt, continuing studies on the OCM mechanism will enable us to develop oxygen carriers that will afford higher selectivities and yields at lower cost.

The reader should recall that oxygen carriers should not only have high reactivity and recyclability but also be robust at high temperatures and have a low monetary cost. By robustness or stability, we mean that the carrier will necessarily adopt different redox states during chemical looping but should not participate in side reactions resulting in other (inactive) states. One method of performance enhancement we have not yet discussed is the introduction of surface dopants[137,138]. For example, one can use spray pyrolysis to prepare alkali-metal-doped Fe_2O_3/Al_2O_3 materials. Doping levels of 5% are enough to hinder Fe–Al phase separation such that the reactivity of the composite is preserved over 50 redox cycles[139]. Likewise, doping 2–10% Ce into $NiO/Ce\text{-}\gamma Al_2O_3$ affords an oxygen carrier that enables improved CO conversions[140]. Furthermore, Zr-doped Cu oxides, prepared by the sol–gel combustion, are good candidates for producing O_2/CO_2 mixtures because O_2 is more readily released when Zr^{4+} ions are present[141]. Moving away from doping small quantities, one can use co-precipitation to prepare CuO-based oxygen carriers stabilized by O-deficient ceria (CeO_{2-x}). CuO comprising 40–50% CeO_{2-x} has threefold higher resistance to C deposition relative to CuO stabilized by Al_2O_3 (REF.[142]).

Even very low concentrations of metal dopants (~1%) can have substantial effects on reactivity. The low levels of doping do not induce phase changes in the oxide but can indeed lower energy barriers associated with activating carbonaceous feedstocks[143]. For example, doping 1% La into Fe_2O_3 has negligible structural effects (FIG. 7a), because only low concentrations are introduced and both metals exist in trivalent states. However, the doping improves redox reactivity while preserving the high oxygen capacity and recyclability. The doped material has 220% the activity of the parent oxide for CO combustion and 178% the activity for CH_4 oxidation (FIG. 7a). One can also perform low-level aliovalent doping by introducing Cu into Fe_2O_3 with the aim of enhancing reactivity towards CH_4. With 1% Cu doping, the CH_4 conversion rate at 700 °C is 570% that of the Fe_2O_3 parent material. The reactivity increase stems from the fact that aliovalent doping also affords oxygen vacancies, the presence of which lowers the barrier to CH_4 activation[144]. These findings exemplify how relatively simple fabrication processes enable low-level doping for high levels of reactivity in metal oxides.

Ni is not only a useful active metal but also a viable dopant material, including in W-based oxygen carriers for the CLPO of CH_4 (REF.[17]) (FIG. 7b). Thus, $Ni_{0.5}WO_x/Al_2O_3$ is superior to WO_3/Al_2O_3 in terms of O availability, CH_4 conversions and syngas yields. The strong interactions between surface-grafted Ni species and WO_x polyhedra accelerate CH_4 activation and the surface partial oxidation reaction. Ex situ X-ray diffraction and in situ infrared spectroscopy were conducted to study the reaction path in the bulk (FIG. 7b, WO_3-WO_2-W-WC) and on the surface (FIG. 7b, CH_4-formyl-CO_2-CO-C), respectively.

Despite the amount of research conducted on modifying oxygen carriers with different dopants and catalysts, much work remains to be done in terms of elucidating surface reaction pathways for various chemical looping applications. The reactions with oxygen carriers involve the generation and transfer of different oxygenic species from the bulk phase to the surface (and vice versa), and they can produce many different products depending on the specific reaction pathways that are operative. Tuning the adsorption energy of organic fragments is important, as is the strength of metal–oxygen bonds, which has a large impact on the distribution and diffusion of various oxygen species. Changes in these energies enable us to modulate product selectivity by favouring certain surface reaction pathways. Strategies such as doping, introducing surface promoters and making use of core–shell structures[123] (FIG. 7c) greatly increase

the chemical space from which we can find an optimal material for a given surface reaction.

Perspectives

Chemical looping enables the simultaneous reaction of feedstocks and separation of products by means of circulating carrier materials. A variety of carrier materials can be used depending on the atoms exchanged in the reactions that make up the overall chemical looping scheme. Oxygen carriers have the potential to be useful in a broad scope of energy and synthesis applications owing to the many reductions and oxidations involved. The outcome of the reactions depends on the oxygen carrier properties, the feedstocks and the reaction conditions. In the reduction step, oxygen carriers are reduced while fuel feedstocks are oxidized. In particular, hydrocarbons can be converted into CO_2/H_2O, CO/H_2 and C2+ chemicals through full, partial and selective oxidation, respectively. In the oxidation step, the oxygen carrier becomes oxidized while a gas is reduced. The lattice oxygen vacancies in the carrier are filled once the carrier removes O atoms from oxidants such as air and CO_2/H_2O, with the release of heat and CO/H_2, respectively. By combining different reduction and oxidation reactions, we can envisage a variety of chemical looping processes that yield clean and efficient power, fuels and other chemicals. Chemical looping has been practised since the end of the 19th century, when we had a particular need for effective chemical conversions that were free of complicated separations. Interest in chemical looping has been renewed because of our present needs for higher efficiency processes for energy conversion and the capture and utilization of CO_2. There has been a recent push towards the design and synthesis of improved oxygen carriers, as well as the engineering of better reactors to enable large-scale demonstrations of the chemical looping approach.

The redox properties of metal oxides can be predicted by considering their equilibrium oxygen potentials. In particular, the p_{O_2} value of a metal oxide can indicate whether it will be useful in CLFO for power and/or heat generation with in situ CO_2 capture. The oxide may instead be better suited to CLPO for syngas and H_2 production or to CLSO as a means to synthesize other chemicals. Several metal oxides reversibly liberate O_2 upon heating, and these materials can be of value for CLOU. In particular, these materials can oxidize even solid fuels at reasonable rates. Although there is always room to engineer better process configurations for a given oxygen carrier, the thermodynamic properties of an oxide are a good starting point from which to select suitable carriers.

We can design an oxygen carrier and know how fast lattice oxygen is delivered to surface catalytic sites. We can thus balance the rates of carrier oxidation and reduction during chemical looping. The formation of CO_x decreases the selectivity of the OCM in conventional flow reactors, as it is prone to undergo non-selective gas-phase combustion that leads to overoxidized products. By contrast, tailored oxygen carriers can afford higher product yields by providing a better distribution of the reactant gas over a bed of carrier particles than is possible in a conventional flow reactor using O_2. The properties of a carrier can also be modified to improve its catalytic function as well as to regulate the rate of reactant diffusion to minimize by-product formation. Thus, in contrast to the typically stoichiometric reactions performed by most oxides, materials featuring catalytic sites can dramatically increase product yield by overcoming product inhibition or kinetic selectivity for an undesired product.

Chemical looping embodies many aspects of materials science and particle technology, including synthesis, reactivity and mechanical properties, flow stability and contact mechanics, and gas–solid reaction engineering. The properties of oxygen carriers used in reduction and oxidation reactions play a particularly important role in chemical looping, which is why we dedicated the majority of this Review to their delineation. Understanding the mechanisms of electron, ion and defect transport, the morphological variations, and the thermodynamic and kinetic properties of these materials is essential if one wants to successfully engineer them for reactive or non-reactive process applications. At present, characterizing the local structures of crystal vacancies using diffraction methods is difficult because these methods yield average structures. By contrast, spectroscopic techniques can be used to study the local structure around dopant atoms but cannot provide structural information beyond the immediate coordination environment of a particular atom. Materials science in general would benefit from having access to characterization techniques for local structure on the subnanometre to nanometre scales, as well as advanced computational tools to further explore reaction dynamics. An important challenge is to develop oxygen carriers whose chemical and physical properties are invariant over many redox cycles. Despite these challenges, we have made substantial recent progress in understanding reaction mechanisms, designing oxygen carrier particles and developing chemical looping reactors. With several pilot-scale and subpilot-scale units now operational across the globe, there can be little doubt that chemical looping technology has the potential to be commercially deployable in the near future for processing CO_2, H_2O and carbonaceous fuels.

Published online: 18 October 2018

1. Fan, L.-S. *Chemical Looping Systems for Fossil Energy Conversions* (Wiley, New York, 2010).
2. Lyngfelt, A. & Linderholm, C. Chemical-looping combustion of solid fuels — status and recent progress. *Energy Procedia* **114**, 371–386 (2017).
3. Boot-Handford, M. E. et al. Carbon capture and storage update. *Energy Environ. Sci.* **7**, 130–189 (2014).
4. Zhao, X. et al. Biomass-based chemical looping technologies: the good, the bad and the future. *Energy Environ. Sci.* **10**, 1885–1910 (2017).
5. Adanez, J., Abad, A., Garcia-Labiano, F., Gayan, P. & de Diego, L. F. Progress in chemical-looping combustion and reforming technologies. *Prog. Energy Combust. Sci.* **38**, 215–282 (2012).
6. Thursfield, A., Murugan, A., Franca, R. & Metcalfe, I. S. Chemical looping and oxygen permeable ceramic membranes for hydrogen production — a review. *Energy Environ. Sci.* **5**, 7421–7459 (2012).
7. Luo, S., Zeng, L. & Fan, L.-S. Chemical looping technology: oxygen carrier characteristics. *Annu. Rev. Chem. Biomol. Eng.* **6**, 53–75 (2015).
8. Buelens, L. C., Galvita, V. V., Poelman, H., Detavernier, C. & Marin, G. B. Super-dry reforming of methane intensifies CO_2 utilization via Le Chatelier's principle. *Science* **354**, 449–452 (2016).
This work demonstrates that oxygen carriers can be used in combination with other carrier materials to enable broader applications of chemical looping technology.
9. Hua, X. & Wang, W. Chemical looping combustion: a new low-dioxin energy conversion technology. *J. Environ. Sci.* **32**, 135–145 (2015).

10. Song, T. et al. Nitrogen transfer of fuel-N in chemical looping combustion. *Combust. Flame* **159**, 1286–1295 (2012).
11. Ishida, M., Zheng, D. & Akehata, T. Evaluation of a chemical-looping–combustion power-generation system by graphic exergy analysis. *Energy* **12**, 147–154 (1987).
12. Dennis, J. S., Müller, C. R. & Scott, S. A. In situ gasification and CO_2 separation using chemical looping with a Cu-based oxygen carrier: performance with bituminous coals. *Fuel* **89**, 2353–2364 (2010).
13. Song, T. & Shen, L. Review of reactor for chemical looping combustion of solid fuels. *Int. J. Greenhouse Gas Control* **76**, 92–110 (2018).
14. Fan, L.-S. *Chemical Looping Partial Oxidation: Gasification, Reforming, and Chemical Syntheses* (Cambridge Univ. Press, Cambridge, 2017).
This book includes comprehensive descriptions of various partial oxidation processes involving chemical looping schemes.
15. Mattisson, T., Lyngfelt, A. & Leion, H. Chemical-looping with oxygen uncoupling for combustion of solid fuels. *Int. J. Greenhouse Gas Control* **3**, 11–19 (2009).
16. Luo, S. et al. Shale gas-to-syngas chemical looping process for stable shale gas conversion to high purity syngas with a H_2: CO ratio of 2: 1. *Energy Environ. Sci.* **7**, 4104–4117 (2014).
17. Chen, S., Zeng, L., Tian, H., Li, X. & Gong, J. Enhanced lattice oxygen reactivity over Ni modified WO_3-based redox catalysts for chemical looping partial oxidation of methane. *ACS Catal.* **7**, 3548–3559 (2017).
This work shows how bulk phase doping and surface modifications of mixed oxides can improve the performances of these oxygen-carrying materials.
18. Mihai, O., Chen, D. & Holmen, A. Chemical looping methane partial oxidation: the effect of the crystal size and O content of $LaFeO_3$. *J. Catal.* **293**, 175–185 (2012).
19. He, F., Galinsky, N. & Li, F. Chemical looping gasification of solid fuels using bimetallic oxygen carrier particles — feasibility assessment and process simulations. *Int. J. Hydrogen Energy* **38**, 7839–7854 (2013).
20. Galvita, V. V., Poelman, H. & Marin, G. B. Hydrogen production from methane and carbon dioxide by catalyst-assisted chemical looping. *Top. Catal.* **54**, 907–913 (2011).
21. Bhavsar, S., Najera, M., Solunke, R. & Veser, G. Chemical looping: to combustion and beyond. *Catal. Today* **228**, 96–105 (2014).
22. Voitic, G. & Hacker, V. Recent advancements in chemical looping water splitting for the production of hydrogen. *RSC Adv.* **6**, 98267–98296 (2016).
23. Jiang, Q. et al. Catalytic function of IrO_x in the two-step thermochemical CO_2-splitting reaction at high temperatures. *ACS Catal.* **6**, 1172–1180 (2016).
24. Muhich, C. L. et al. Efficient generation of H_2 by splitting water with an isothermal redox cycle. *Science* **341**, 540–542 (2013).
25. Zhang, J., Haribal, V. & Li, F. Perovskite nanocomposites as effective CO_2-splitting agents in a cyclic redox scheme. *Sci. Adv.* **3**, e1701184 (2017).
26. Contractor, R. M. Dupont's CFB technology for maleic anhydride. *Chem. Eng. Sci.* **54**, 5627–5632 (1999).
27. Patience, G. S. & Bockrath, R. E. Butane oxidation process development in a circulating fluidized bed. *Appl. Catal., A* **376**, 4–12 (2010).
28. Naeem, M. A. et al. Optimization of the structural characteristics of CaO and its effective stabilization yield high-capacity CO_2 sorbents. *Nat. Comm.* **9**, 2408 (2018).
29. Brunet, S., Mey, D., Pérot, G., Bouchy, C. & Diehl, F. On the hydrodesulfurization of FCC gasoline: a review. *Appl. Catal., A* **278**, 143–172 (2005).
30. Michalsky, R., Avram, A. M., Peterson, B. A., Pfromm, P. H. & Peterson, A. A. Chemical looping of metal nitride catalysts: low-pressure ammonia synthesis for energy storage. *Chem. Sci.* **6**, 3965–3974 (2015).
31. Laassiri, S., Zeinalipour-Yazdi, C. D., Catlow, C. R. A. & Hargreaves, J. S. J. The potential of manganese nitride based materials as nitrogen transfer reagents for nitrogen chemical looping. *Appl. Catal., B* **223**, 60–66 (2018).
32. Hepworth, T. C. Oxygen for limelight. *Nature* **47**, 176–177 (1892).
33. Hardie, D. W. F. & Pratt, J. D. *A History of the Modern British Chemical Industry* (Pergamon Press, Oxford, 1966).
34. Bergmann, F. J. Process for the production of calcium carbide in blast furnaces. German patent 29384 (1897).
35. Lewis, W. K. & Gilliland, E. R. Conversion of hydrocarbons with suspended catalyst. US Patent 2498088 (1950).
36. Lewis, W. K. & Gilliland, E. R. Production of pure carbon dioxide. US Patent 2665971 (1954).
37. Institute of Gas Technology. *Development of the Steam-Iron Process for Hydrogen Production* (US Department Energy, 1979).
38. Richter, H. J. & Knoche, K. F. Reversibility of combustion processes. *ACS Symp. Ser.* **235**, 71–85 (1983).
39. Ströhle, J., Orth, M. & Epple, B. Design and operation of a $1MW_{th}$ chemical looping plant. *Appl. Energy* **113**, 1490–1495 (2014).
40. Whitty, K., Lighty, J. & Fry, A. *Development and Scale-Up of Copper-Based Chemical Looping with Oxygen Uncoupling. Presented at the 4th International Conference on Chemical Looping* (Nanjing, China, 2016).
41. Langorgen, O., Saanum, I. & Haugen, N. E. L. *Performance of a 150 kW Chemical Looping Combustion Reactor System for Gaseous Fuels Using a Copper-Based Oxygen Carrier. Presented at the 4th International Conference on Chemical Looping* (Nanjing, China, 2016).
42. Andrus, H. E., Brautsch, A. & Beal, C. Alstom's chemical looping coal-fired power plant development program. *Proc. Int. Tech. Conf. Coal Util. Fuel Syst.* **2**, 993–1004 (2007).
43. Fan, L.-S. *Chemical Looping Technology for Combustion, Gasification, Reforming, and Chemical Syntheses: Redox Reaction Mechanism and Technology Commercialization Readiness. Presented at the 255th National Meeting and Exposition of the American-Chemical-Society* (New Orleans, USA, 2018).
44. Corcoran, A., Knutsson, P., Lind, F. & Thunman, H. Comparing the structural development of sand and rock ilmenite during long-term exposure in a biomass fired 12MWth CFB-boiler. *Fuel Process. Technol.* **171**, 39–44 (2018).
45. Shen, L. H. *3MWth Pilot Demonstration of Chemical Looping Combustion and Gasification of Coal in China. Presented at the 6th International Conference on CO2 Emission Control and Utilization* (Hangzhou, China, 2018).
46. Li, Z. S. *Demonstration of CLC Technology in Semi-Industrial Scale via a Chinese-European Collaboration. Presented at the 6th International Conference on CO2 Emission Control and Utilization* (Hangzhou, China, 2018).
47. Lane, H. Process of producing hydrogen. US Patent 1078686 (1913).
48. Reed, H. C. & Berg, C. H. Hydrogen. US Patent 2635947 (1953).
49. Dobbyn, R. C. et al. *Evaluation of the Performance of Materials and Components Used in the CO2 Acceptor Process Gasification Pilot Plant* (US Department Energy, 1978).
50. Rao, C. N. R. & Dey, S. Solar thermochemical splitting of water to generate hydrogen. *Proc. Natl Acad. Sci. USA* **114**, 13385–13393 (2017).
51. Muhich, C. L. et al. A review and perspective of efficient hydrogen generation via solar thermal water splitting. *WIREs Energy Environ.* **5**, 261–287 (2016).
52. Haribal, V. P., He, F., Mishra, A. & Li, F. Iron-doped $BaMnO_3$ for hybrid water splitting and syngas generation. *ChemSusChem* **10**, 3402–3408 (2017).
53. Otsuka, K., Wang, Y., Sunada, E. & Yamanaka, I. Direct partial oxidation of methane to synthesis gas by cerium oxide. *J. Catal.* **175**, 152–160 (1998).
54. Steinfeld, A., Kuhn, P. & Karni, J. High-temperature solar thermochemistry: production of iron and synthesis gas by Fe_3O_4-reduction with methane. *Energy* **18**, 239–249 (1993).
55. Zheng, Y. et al. Designed oxygen carriers from macroporous $LaFeO_3$ supported CeO_2 for chemical-looping reforming of methane. *Appl. Catal., B* **202**, 51–63 (2017).
56. Zhao, K. et al. Exploration of the mechanism of chemical looping steam methane reforming using double perovskite-type oxides $La_{1.6}Sr_{0.4}FeCoO_6$. *Appl. Catal., B* **219**, 672–682 (2017).
57. Kulkarni, P. et al. *Fuel-Flexible Gasification-Combustion Technology for Production of H2 and Sequestration-Ready CO2* (US Department Energy, 2008).
58. Jia, Z. et al. *Design Basis of 1 MWth Calcium Looping Gasification Pilot Unit. Presented at the 2018 International Pittsburgh Coal Conference* (Xuzhou, China, 2018).
59. Chung, C., Qin, L., Shah, V. & Fan, L.-S. Chemically and physically robust, commercially-viable iron-based composite oxygen carriers sustainable over 3000 redox cycles at high temperatures for chemical looping applications. *Energy Environ. Sci.* **10**, 2318–2323 (2017).
60. Fan, L.-S., Zeng, L., Wang, W. & Luo, S. Chemical looping processes for CO_2 capture and carbonaceous fuel conversion — prospect and opportunity. *Energy Environ. Sci.* **5**, 7254–7280 (2012).
61. Zeng, L., Kathe, M. V., Chung, E. Y. & Fan, L.-S. Some remarks on direct solid fuel combustion using chemical looping processes. *Curr. Opin. Chem. Eng.* **1**, 290–295 (2012).
62. Qin, L. et al. Nanostructure formation mechanism and ion diffusion in iron–titanium composite materials with chemical looping redox reactions. *J. Mater. Chem. A* **3**, 11302–11312 (2015).
This paper details ionic diffusion in a mixed-oxide system and how this is related to morphology changes during chemical looping processes.
63. Cavani, F. & Trifirò, F. The oxidative dehydrogenation of ethane and propane as an alternative way for the production of light olefins. *Catal. Today* **24**, 307–313 (1995).
64. Keller, G. E. & Bhasin, M. M. Synthesis of ethylene via oxidative coupling of methane: I. Determination of active catalysts. *J. Catal.* **73**, 9–19 (1982).
65. Neal, L. M., Yusuf, S., Sofranko, J. A. & Li, F. Oxidative dehydrogenation of ethane: a chemical looping approach. *Energy Technol.* **4**, 1200–1208 (2016).
66. Chung, E. Y. et al. Catalytic oxygen carriers and process systems for oxidative coupling of methane using the chemical looping technology. *Ind. Eng. Chem. Res.* **55**, 12750–12764 (2016).
67. Brady, C., Murphy, B. & Xu, B. Enhanced methane dehydroaromatization via coupling with chemical looping. *ACS Catal.* **7**, 3924–3928 (2017).
68. Sushkevich, V. L., Palagin, D., Ranocchiari, M. & van Bokhoven, J. A. Selective anaerobic oxidation of methane enables direct synthesis of methanol. *Science* **356**, 523–527 (2017).
This work describes the potential application of chemical looping processes in the direct syntheses of chemicals from simple feedstocks.
69. Grasselli, R. K., Stern, D. L. & Tsikoyiannis, J. G. Catalytic dehydrogenation (DH) of light paraffins combined with selective hydrogen combustion (SHC): I. DH SHC DH catalysts in series (co-fed process mode). *Appl. Catal., A* **189**, 1–8 (1999).
70. Grasselli, R. K., Stern, D. L. & Tsikoyiannis, J. G. Catalytic dehydrogenation (DH) of light paraffins combined with selective hydrogen combustion (SHC): II. DH+SHC catalysts physically mixed (redox process mode). *Appl. Catal., A* **189**, 9–14 (1999).
71. Mamedov, E. A. & Cortés Corberán, V. Oxidative dehydrogenation of lower alkanes on vanadium oxide-based catalysts. The present state of the art and outlooks. *Appl. Catal., A* **127**, 1–40 (1995).
72. Al-Ghamdi, S. A. & de Lasa, H. I. Propylene production via propane oxidative dehydrogenation over VO_x/γ-Al_2O_3 catalyst. *Fuel* **128**, 120–140 (2014).
73. Gao, Y., Neal, L. M. & Li, F. Li-promoted $La_xSr_{2-x}FeO_{4-\delta}$ core–shell redox catalysts for oxidative dehydrogenation of ethane under a cyclic redox scheme. *ACS Catal.* **6**, 7293–7302 (2016).
74. Yusuf, S., Neal, L. M. & Li, F. Effect of promoters on manganese-containing mixed metal oxides for oxidative dehydrogenation of ethane via a cyclic redox scheme. *ACS Catal.* **7**, 5163–5173 (2017).
75. Yusuf, S. et al. Manganese silicate based redox catalysts for greener ethylene production via chemical looping — oxidative dehydrogenation of ethane. *Appl. Catal., B* **232**, 77–85 (2018).
76. Novotný, P., Yusuf, S., Li, F. & Lamb, H. H. Oxidative dehydrogenation of ethane using MoO_3/Fe_2O_3 catalysts in a cyclic redox mode. *Catal. Today*. https://doi.org/10.1016/j.cattod.2018.02.046 (2018).
77. Gao, Y., Haeri, F., He, F. & Li, F. Alkali metal-promoted $La_xSr_{2-x}FeO_{4-\delta}$ redox catalysts for chemical looping oxidative dehydrogenation of ethane. *ACS Catal.* **8**, 1757–1766 (2018).
78. Chan, M. S. C., Marek, E., Scott, S. A. & Dennis, J. S. Chemical looping epoxidation. *J. Catal.* **359**, 1–7 (2018).
79. Chan, M. S. C. et al. Improving hydrogen yields, and hydrogen:steam ratio in the chemical looping production of hydrogen using $Ca_2Fe_2O_5$. *Chem. Eng. J.* **296**, 406–411 (2016).
80. Zhao, K. et al. Perovskite-type oxides $LaFe_{1-x}Co_xO_3$ for chemical looping steam methane reforming to syngas and hydrogen co-production. *Appl. Energy* **168**, 193–203 (2016).
81. Rydén, M. et al. Novel oxygen-carrier materials for chemical-looping combustion and chemical-looping

reforming; $La_xSr_{1-x}Fe_yCo_{1-y}O_{3-\delta}$ perovskites and mixed-metal oxides of NiO, Fe_2O_3 and Mn_3O_4. *Int. J. Greenhouse Gas Control* **2**, 21–36 (2008).
82. Fan, L.-S., Tong, A. & Zeng, L. in *Multiphase Reactor Engineering for Clean and Low–Carbon Energy Applications* (eds Cheng, Y., Wei, F. & Jin, Y.) 377–400 (Wiley, 2017).
83. Imtiaz, Q., Hosseini, D. & Müller, C. R. Review of oxygen carriers for chemical looping with oxygen uncoupling (CLOU): thermodynamics, material development, and synthesis. *Energy Technol.* **1**, 633–647 (2013).
84. Lau, C. Y., Dunstan, M. T., Hu, W., Grey, C. P. & Scott, S. A. Large scale in silico screening of materials for carbon capture through chemical looping. *Energy Environ. Sci.* **10**, 818–831 (2017).
This paper describes how advanced computational tools can be used for the screening of new potential oxygen carriers.
85. Adánez, J. et al. Selection of oxygen carriers for chemical-looping combustion. *Energy Fuels* **18**, 371–377 (2004).
86. Andersson, D. A., Simak, S. I., Skorodumova, N. V., Abrikosov, I. A. & Johansson, B. Optimization of ionic conductivity in doped ceria. *Proc. Natl Acad. Sci. USA* **103**, 3518–3521 (2006).
87. Kümmerle, E. A. & Heger, G. The Structures of C–$Ce_2O_{3+\delta}$, Ce_7O_{12}, and $Ce_{11}O_{20}$. *J. Solid State Chem.* **147**, 485–500 (1999).
88. Yang, Z., Woo, T. K., Baudin, M. & Hermansson, K. Atomic and electronic structure of unreduced and reduced CeO_2 surfaces: a first-principles study. *J. Chem. Phys.* **120**, 7741–7749 (2004).
89. Nolan, M., Parker, S. C. & Watson, G. W. The electronic structure of oxygen vacancy defects at the low index surfaces of ceria. *Surf. Sci.* **595**, 223–232 (2005).
90. Cheng, Z., Sherman, B. J. & Lo, C. S. Carbon dioxide adsorption and activation on ceria (110): a density functional theory study. *J. Chem. Phys.* **138**, 014702 (2013).
91. Paier, J., Penschke, C. & Sauer, J. Oxygen defects and surface chemistry of ceria: quantum chemical studies compared to experiment. *Chem. Rev.* **113**, 3949–3985 (2013).
92. Mahato, N., Banerjee, A., Gupta, A., Omar, S. & Balani, K. Progress in material selection for solid oxide fuel cell technology: a review. *Prog. Mater. Sci.* **72**, 141–337 (2015).
93. Dai, X. P., Li, R. J., Yu, C. C. & Hao, Z. P. Unsteady-state direct partial oxidation of methane to synthesis gas in a fixed-bed reactor using $AFeO_3$ (A=La, Nd, Eu) perovskite-type oxides as oxygen storage. *J. Phys. Chem. B* **110**, 22525–22531 (2006).
94. Mihai, O., Chen, D. & Holmen, A. Catalytic consequence of oxygen of lanthanum ferrite perovskite in chemical looping reforming of methane. *Ind. Eng. Chem. Res.* **50**, 2613–2621 (2011).
95. Nalbandian, L., Evdou, A. & Zaspalis, V. $La_{1-x}Sr_xM_yFe_{1-y}O_{3-\delta}$ perovskites as oxygen-carrier materials for chemical-looping reforming. *Int. J. Hydrogen Energy* **36**, 6657–6670 (2011).
96. Pineau, A., Kanari, N. & Gaballah, I. Kinetics of reduction of iron oxides by H_2: part I: low temperature reduction of hematite. *Thermochim. Acta* **447**, 89–100 (2006).
97. Pineau, A., Kanari, N. & Gaballah, I. Kinetics of reduction of iron oxides by H_2: part II. Low temperature reduction of magnetite. *Thermochim. Acta* **456**, 75–88 (2007).
98. Thomas, T., Fan, L.-S., Gupta, P. & Velazquez-Vargas, L. G. Combustion looping using composite oxygen carriers. US Patent 7767191 (2003).
99. Tong, A., Zeng, L., Kathe, M. V., Sridhar, D. & Fan, L.-S. Application of the moving-bed chemical looping process for high methane conversion. *Energy Fuels* **27**, 4119–4128 (2013).
100. Cheng, Z. et al. Methane adsorption and dissociation on iron oxide oxygen carriers: the role of oxygen vacancies. *Phys. Chem. Chem. Phys.* **18**, 16423–16435 (2016).
101. Hsia, C., Pierre, G. R. St., Raghunathan, K. & Fan, L.-S. Diffusion through $CaSO_4$ formed during the reaction of CaO with SO_2 and O_2. *AIChE J.* **39**, 698–700 (1993).
102. Hsia, C., Pierre, G. R. S. & Fan, L.-S. Isotope study on diffusion in $CaSO_4$ formed during sorbent-flue-gas reaction. *AIChE J.* **41**, 2337–2340 (1995).
103. Ando, K. & Oishi, Y. Self-diffusion coefficients of oxygen ion in single crystals of $MgO \cdot nAl_2O_3$ spinels. *J. Chem. Phys.* **61**, 625–629 (1974).
104. Oishi, Y. & Ando, K. Self-diffusion of oxygen in polycrystalline $MgAl_2O_4$. *J. Chem. Phys.* **63**, 376–378 (1975).
105. Reddy, K. P. R. & Cooper, A. R. Oxygen diffusion in MgO and α-Fe_2O_3. *J. Am. Ceram. Soc.* **66**, 664–666 (1983).
106. Uberuaga, B. P. et al. Defect kinetics in spinels: long-time simulations of $MgAl_2O_4$, $MgGa_2O_4$, and $MgIn_2O_4$. *Phys. Rev. B* **75**, 104116 (2007).
107. Wilson, C. et al. Structure and properties of ilmenite from first principles. *Phys. Rev. B* **71**, 075202 (2005).
108. Sun, Z., Luo, S. & Fan, L.-S. Ionic transfer mechanism of COS reaction with CaO: inert marker experiment and density functional theory (DFT) calculation. *AIChE J.* **58**, 2617–2620 (2012).
109. Nakamura, R., Tokozakura, D., Nakajima, H., Lee, J. G. & Mori, H. Hollow oxide formation by oxidation of Al and Cu nanoparticles. *J. Appl. Phys.* **101**, 074303 (2007).
110. Qin, L., Majumder, A., Fan, J. A., Kopechek, D. & Fan, L.-S. Evolution of nanoscale morphology in single and binary metal oxide microparticles during reduction and oxidation processes. *J. Mater. Chem. A* **2**, 17511–17520 (2014).
111. Fu, Y., Chen, J. & Zhang, H. Synthesis of Fe_2O_3 nanowires by oxidation of iron. *Chem. Phys. Lett.* **350**, 491–494 (2001).
112. Wen, X., Wang, S., Ding, Y., Wang, Z. L. & Yang, S. Controlled growth of large-area, uniform, vertically aligned arrays of α-Fe_2O_3 nanobelts and nanowires. *J. Phys. Chem. B* **109**, 215–220 (2005).
113. Dang, H. Y., Wang, J. & Fan, S. S. The synthesis of metal oxide nanowires by directly heating metal samples in appropriate oxygen atmospheres. *Nanotechnology* **14**, 738 (2003).
114. He, F., Wei, Y., Li, H. & Wang, H. Synthesis gas generation by chemical-looping reforming using Ce-based oxygen carriers modified with Fe, Cu, and Mn oxides. *Energy Fuels* **23**, 2095–2102 (2009).
115. Li, F. et al. Syngas chemical looping gasification process: oxygen carrier particle selection and performance. *Energy Fuels* **23**, 4182–4189 (2009).
116. Azimi, G., Mattisson, T., Leion, H., Rydén, M. & Lyngfelt, A. Comprehensive study of Mn–Fe–Al oxygen-carriers for chemical-looping with oxygen uncoupling (CLOU). *Int. J. Greenhouse Gas Control* **34**, 12–24 (2015).
117. de Diego, L. F. et al. Synthesis gas generation by chemical-looping reforming in a batch fluidized bed reactor using Ni-based oxygen carriers. *Chem. Eng. J.* **144**, 289–298 (2008).
118. Qin, L., Cheng, Z., Guo, M., Fan, J. A. & Fan, L.-S. Morphology evolution and nanostructure of chemical looping transition metal oxide materials upon redox processes. *Acta Mater.* **124**, 568–578 (2017).
119. Shafiefarhood, A., Zhang, J., Neal, L. M. & Li, F. Rh-promoted mixed oxides for "low-temperature" methane partial oxidation in the absence of gaseous oxidants. *J. Mater. Chem. A* **5**, 11930–11939 (2017).
120. Jin, Y., Sun, C. & Su, S. Experimental and theoretical study of the oxidation of ventilation air methane over Fe_2O_2 and CuO. *Phys. Chem. Chem. Phys.* **17**, 16277–16284 (2015).
121. Cheng, Z. et al. Oxygen vacancy promoted methane partial oxidation over iron oxide oxygen carriers in the chemical looping process. *Phys. Chem. Chem. Phys.* **18**, 32418–32428 (2016).
122. Neal, L. M., Shafiefarhood, A. & Li, F. Dynamic methane partial oxidation using a Fe_2O_3@$La_{0.8}Sr_{0.2}FeO_{3-\delta}$ core–shell redox catalyst in the absence of gaseous oxygen. *ACS Catal.* **4**, 3560–3569 (2014).
This work describes a new core–shell catalytic oxygen carrier and the mechanism by which it converts methane into syngas.
123. Shafiefarhood, A., Galinsky, N., Huang, Y., Chen, Y. & Li, F. Fe_2O_3@$La_xSr_{1-x}FeO_3$ core–shell redox catalyst for methane partial oxidation. *ChemCatChem* **6**, 790–799 (2014).
124. Liss, W. E. Impacts of shale gas advancements on natural gas utilization in the United States. *Energy Technol.* **2**, 953–967 (2014).
125. Fleischer, V. et al. Investigation of the role of the Na_2WO_4/Mn/SiO_2 catalyst composition in the oxidative coupling of methane by chemical looping experiments. *J. Catal.* **360**, 102–117 (2018).
126. Borchert, H. & Baerns, M. The effect of oxygen-anion conductivity of metal–oxide doped lanthanum oxide catalysts on hydrocarbon selectivity in the oxidative coupling of methane. *J. Catal.* **168**, 315–320 (1997).
127. Cheng, Z. & Lo, C. S. Effect of support structure and composition on the catalytic activity of Pt nanoclusters for methane dehydrogenation. *Ind. Eng. Chem. Res.* **52**, 15447–15454 (2013).
128. Liu, S., Tan, X., Li, K. & Hughes, R. Methane coupling using catalytic membrane reactors. *Catal. Rev.* **43**, 147–198 (2001).
129. Voskresenskaya, E. N., Roguleva, V. G. & Anshits, A. G. Oxidant activation over structural defects of oxide catalysts in oxidative methane coupling. *Catal. Rev.* **37**, 101–143 (1995).
130. Malekzadeh, A. et al. Correlation of electrical properties and performance of OCM MO_x/Na_2WO_4/SiO_2 catalysts. *Catal. Commun.* **2**, 241–247 (2001).
131. Greish, A. A. et al. Oxidative coupling of methane in the redox cyclic mode over the catalysts on the basis of CeO_2 and La_2O_3. *Mendeleev Commun.* **20**, 28–30 (2010).
132. Sung, J. S. et al. Peculiarities of oxidative coupling of methane in redox cyclic mode over Ag–La_2O_3/SiO_2 catalysts. *Appl. Catal., A* **380**, 28–32 (2010).
133. Huang, K., Zhan, X.-L., Chen, F.-Q. & Lü, D.-W. Catalyst design for methane oxidative coupling by using artificial neural network and hybrid genetic algorithm. *Chem. Eng. Sci.* **58**, 81–87 (2003).
134. Chua, Y. T., Mohamed, A. R. & Bhatia, S. Oxidative coupling of methane for the production of ethylene over sodium-tungsten-manganese-supported-silica catalyst (Na-W-Mn/SiO_2). *Appl. Catal., A* **343**, 142–148 (2008).
135. Hou, Y.-H., Han, W.-C., Xia, W.-S. & Wan, H.-L. Structure sensitivity of $La_2O_2CO_3$ catalysts in the oxidative coupling of methane. *ACS Catal.* **5**, 1663–1674 (2015).
136. Cheng, Z. et al. C_2 selectivity enhancement in chemical looping oxidative coupling of methane over a Mg–Mn composite oxygen carrier by Li-doping-induced oxygen vacancies. *ACS Energy Lett.* **3**, 1730–1736 (2018).
137. Cao, Y., Sit, S. P. & Pan, W.-P. Preparation and characterization of lanthanum-promoted copper-based oxygen carriers for chemical looping combustion process. *Aerosol Air Qual. Res.* **14**, 572–584 (2014).
138. Cao, Y., Zhao, H.-Y., Sit, S. P. & Pan, W.-P. Lanthanum-promoted copper-based oxygen carriers for chemical looping combustion process. *J. Therm. Anal. Calorim.* **116**, 1257–1266 (2014).
139. Liu, L. & Zachariah, M. R. Enhanced performance of alkali metal doped Fe_2O_3 and Fe_2O_3/Al_2O_3 composites as oxygen carrier material in chemical looping combustion. *Energy Fuels* **27**, 4977–4983 (2013).
140. Mohamed, S. A., Quddus, M. R., Razzak, S. A., Hossain, M. M. & de Lasa, H. I. Fluidizable NiO/Ce-γAl_2O_3 oxygen carrier for chemical looping combustion. *Energy Fuels* **29**, 6095–6103 (2015).
141. Wang, M., Liu, J., Hu, J. & Liu, F. O_2–CO_2 mixed gas production using a Zr-doped Cu-based oxygen carrier. *Ind. Eng. Chem. Res.* **54**, 9805–9812 (2015).
142. Imtiaz, Q., Kurlov, A., Rupp, J. L. M. & Müller, C. R. Highly efficient oxygen-storage material with intrinsic coke resistance for chemical looping combustion-based CO_2 capture. *ChemSusChem* **8**, 2055–2065 (2015).
143. Qin, L. et al. Impact of 1% lanthanum dopant on carbonaceous fuel redox reactions with an iron-based oxygen carrier in chemical looping processes. *ACS Energy Lett.* **2**, 70–74 (2017).
This article discloses how very low concentrations of a metal oxide dopant can lower the energy barrier for C–H bond activation.
144. Qin, L. et al. Enhanced methane conversion in chemical looping partial oxidation systems using a copper doping modification. *Appl. Catal., B* **235**, 143–149 (2018).
145. Chroneos, A., Yildiz, B., Tarancón, A., Parfitt, D. & Kilner, J. A. Oxygen diffusion in solid oxide fuel cell cathode and electrolyte materials: mechanistic insights from atomistic simulations. *Energy Environ. Sci.* **4**, 2774–2789 (2011).

Acknowledgements
L.Z. and J.G. thank the National Key R&D Program of China (2016YFB0600901), the National Natural Science Foundation of China (Grants 21525626 and U1663224) and the Program of Introducing Talents of Discipline to Universities of China (Grant B06006). J.A.F. acknowledges support from the US National Science Foundation (Grant 1804224) and the Packard Fellowship Foundation. Z.C. and L.-S.F. thank the US National Science Foundation (Grant 1236467), Ohio State University (funding from the C. John Easton Professorship in Engineering) and the Ohio Supercomputer Center.

Author contributions
All authors contributed equally to the preparation of this manuscript.

Competing interests
The authors declare no competing interests.